University of Arkansas, Fayetteville

ScholarWorks@UARK

Chemistry & Biochemistry Undergraduate Honors Theses

Chemistry & Biochemistry

5-2020

The Development and Evaluation of Alginate Nanofibers as a Neuroprotective Nano-scaffold for Amyotrophic Lateral Sclerosis (ALS)

Julia Bielanin

Follow this and additional works at: https://scholarworks.uark.edu/chbcuht

 Part of the Macromolecular Substances Commons, and the Therapeutics Commons

Citation

Bielanin, J. (2020). The Development and Evaluation of Alginate Nanofibers as a Neuroprotective Nano-scaffold for Amyotrophic Lateral Sclerosis (ALS). *Chemistry & Biochemistry Undergraduate Honors Theses* Retrieved from https://scholarworks.uark.edu/chbcuht/26

This Thesis is brought to you for free and open access by the Chemistry & Biochemistry at ScholarWorks@UARK. It has been accepted for inclusion in Chemistry & Biochemistry Undergraduate Honors Theses by an authorized administrator of ScholarWorks@UARK. For more information, please contact ccmiddle@uark.edu.

The Development and Evaluation of Alginate Nanofibers as a Neuroprotective Nano-scaffold for Amyotrophic Lateral Sclerosis (ALS)

An Honors Thesis submitted in partial fulfillment
of the requirements for Honors Studies in Chemistry with a focus in Biochemistry

2020

Chemistry
J. William Fulbright College of Arts and Sciences
The University of Arkansas
Julia Bielanin

Table of Contents

Abstract

Amyotrophic lateral sclerosis (ALS) is a progressive, fatal neurodegenerative disorder characterized in pathology by a significant loss of upper and lower motor neurons, leading to muscle wasting and loss of voluntary movement. There are about 6,000-8,000 new cases of ALS diagnosed per year in the U.S., with a fatal outcome within 2 to 4 years (on average) after diagnosis. There are only two FDA approved drugs for treating ALS. Both are very expensive and only have modest benefits for patients. The population is in dire need of more affordable and effective medicine for the treatment of ALS.

Therefore, the goal of this research was to test the viability of alginate nanofibers cross-linked to non-toxic levels of calcium, barium, and strontium for the release of methylene blue as a potential novel drug delivery system for the treatment of ALS. Alginate possesses antioxidant activity, immunoregulatory activity, anti-inflammatory activity, and neuroprotective activity. Methylene blue also possesses antioxidant activity and has been shown to inhibit aggregation of TDP43, a protein that is aggregated in up to 97% of all ALS patients. These properties, in combination, would have great advantages for mitigating the multi-faceted pathogenesis of amyotrophic lateral sclerosis.

The nanofibers were synthesized using immersive rotary jet spinning followed by lyophilization. Various concentrations (50 mM, 100 mM, 200 mM, 300 mM, and 400 mM) of cross-linking cation were used to cross-link with 1% w/v alginate solution. Release studies with methylene blue occurred over a three-hour time period. Data were collected on the loading efficiencies, release profiles, and degradation times of the nanofibers using UV-Vis spectroscopy. Strontium 300 mM loaded with 31.2 μL of methylene blue had the highest loading efficiency at 59.9%. This nanofiber also loaded the most moles per milligram of nanofiber at 2.9 nanomoles/mg. Barium alginate nanofibers had the highest structural integrity followed by strontium then calcium. The release

kinetics of the nanofibers were inconclusive due to high error associated with each time point potentially due to redox reactions between alginate and methylene blue.

Introduction

Amyotrophic Lateral Sclerosis (ALS) is a progressive neurodegenerative disorder that is part of a wider group of disorders known as motor neuron diseases.[1] Motor neuron diseases (MNDs) are characterized by the gradual deterioration, dysfunction, and death of motor neurons.[2] Along with ALS, progressive bulbar palsy, primary lateral sclerosis, Kennedy's disease, and a few others are classified as MNDs.[2] MNDs are categorized on several dimensions. The first is overarching etiology: inherited or sporadic.[2] For ALS, inherited or familial ALS accounts for approximately 5-10% of all cases, whereas, approximately 90% of cases are considered sporadic.[3]

The second dimension MNDs are categorized by are the neurons that are primarily affected.[2] Motor neuron diseases can effecting upper, lower, or both types of motor neurons.[2] Classical ALS affects both the upper motor neurons, the neurons in the cerebral cortex that activate interneurons and lower motor neurons, and lower motor neurons, the neurons that directly signal muscles to contract or relax.[2] The third category relates to the muscle group that symptoms initiate in. For ALS, symptoms start primarily in the limbs or bulbar (affecting muscles of the head and neck).[4] Approximately 66% of ALS patients have spinal/limb onset and 34% have a bulbar onset. [4] Early symptoms of spinal/limb onset ALS include muscle weakness or stiffness, tripping more than normal, and fasciculations.[1] Whereas, early symptoms of bulbar onset ALS include difficulty chewing or swallowing, slurred speech (dysarthria), and difficulty breathing (dyspnea).[1] The disease progresses to eventually affect all muscles needed to move, eat, speak and breathe.[5] As the disease progresses about 50% of patients with ALS experience

cognitive or behavioral changes on the spectrum of frontotemporal dementia with apathy and loss of sympathy among the most common of behavioral symptoms.[6] Eventually, ALS patients die of respiratory failure typically 2-4 years after the onset of symptoms.[7] There is no cure for ALS at this point.

Prevalence and Incidence of ALS

The global crude prevalence of ALS is 4.42 per 100,000 people, meaning roughly 4 people out of every 100,000 people are affected by ALS.[8] The global incidence is 1.59 per 100,000 people per year.[8] This translates to 2 people out of every 100,000 people diagnosed each year globally. The incidence and prevalence of males are higher than those in females.[7] Possible reasons for the differences in prevalence and incidence of ALS between women and men include different exposures to toxins and different biological responses to the toxins.[9] It is also possible that there are underlying differences between male and female nervous systems in how they repair damage.[9] However, this has not been definitively determined.[9] The incidence also grows by age globally with a peak at 60-70 years old.[8]

In the United States, the prevalence of ALS is different than in other regions of the world.[10] The prevalence is about 5.0 cases per 100,000 in the United States with the prevalence in Caucasians (5.4) more than twice of that observed in African Americans (2.4).[10] Both prevalence and incidence are lowest in South Asia, however, the age of onset is much earlier.[8] The longest survival times post-diagnosis are also observed in South Asia.[8] Developed regions have higher prevalence and incidence compared to developing or undeveloped regions.[8] The observed difference in incidence may be due to the fact that developed regions have a higher mean age than developing regions.[8]

Several other factors besides geographical region have been identified as associated with ALS incidence and prevalence. In a study conducted by the NIH, occupations associated with higher socioeconomic status experienced greater ALS disease mortality.[11] These occupations included mathematics, architecture, engineering, law, and education.[11] Clustering of ALS has also been reported among American football players, Italian soccer players, and United States military veterans.[12–14] It is thought that the four-fold increase of prevalence in American football players is due to strenuous physical activity and increased head injury, however, it could also be due to misdiagnosis of chronic traumatic encephalopathy.[12] In a case-controlled study comparing road cyclists, professional basketball players, and professional soccer players only the soccer players displayed higher mortality due to ALS suggesting that the risk is not related to physical activity per se.[14] Exposure to chemicals such as toxic herbicides or fertilizers as well as increased frequency of head injuries are theorized to be the cause of increased prevalence in soccer players.[15]

Many studies have investigated environmental risk factors for ALS including exposures to solvents, degreasers, alcohols, insecticides, fertilizers, heavy metals, and pesticides because of their potential to explain sporadic ALS which accounts for the majority of ALS cases.[15–17] Overall, agricultural chemicals and pesticides have been repeatedly linked but have been based on poor methodology and self-report.[17] Smoking, however, has been associated with an increased risk of ALS.[18] There is a 9% increase in risk for every 10 years of smoking and a 10% increase for each additional 10 cigarettes smoked per day.[18] This increase in risk could be due to direct neurotoxic effect on motor neurons or by increasing oxidative stress.[18] The increased prevalence observed in United States military personnel could be due to increased exposure to detrimental lifestyle factors (e.g. smoking) and the increased proportion of men (96%).[16] Other

military-specific exposures have been actively explored such as emotional/psychological trauma, exposure to transmissible agents, and physical trauma, however, there is not strong evidence that any particular military exposure serves as a risk factor for the increased mortality from ALS that is observed.[16]

ALS cases are projected to increase by 69% in the next 20 years.[19] This disease will continue to impact human lives at an increasingly larger scale due to the aging of the world's population, improving healthcare, and economic conditions.[19] Additionally, ALS is of increasing interest to the general population because of its high social impact. This is reflected by ALS being the 3rd most googled neurological disease in the United States in 2015.[20] ALS also has a high economic impact. The economic burden results from the combination of frequent hospital admissions, rehabilitation, health care transport, medications, medical tests and examinations, reduction of working time, skilled home care, and early retirements.[21] The total annual cost per patient with ALS is $69,475 in the US, $59,018 in Spain, and $47,092 in Germany.[19,21,22] The costs increase with disease progression and not only reduce the patients' quality of life but also the quality life of the caretakers.[21,22]

The Etiology of ALS

The etiology of the disease is just as enigmatic as the patterns of incidence and prevalence seen globally. Considerable progress has been made in unraveling the genetic etiology of ALS by identifying underlying genes. These genes include SOD1, TARDBP, FUS, OPTN, VCP, UBQLN2, C9ORF72 and PFN1.[23] In combination, these genes explain 75% of familial cases and 11% of sporadic cases.[23] Identifying the genetic etiology of ALS provides fundamental insights into the cellular mechanisms underlying neuron degeneration with each new gene providing another clue to the complexities of ALS. Superoxide dismutase 1's (SOD1)

relation to ALS was discovered in 1993.[24] This discovery lead to the development of the SOD1 transgenic mouse model and opened research to the potential implication of oxygen free radicals as a pathogenetic mechanism for motor neuron death in familial and sporadic ALS.[24]

However, human SOD1 ALS is thought to be distinct from that of other types of ALS because it lacks TDP43 and/or FUS pathology, two features that are present in nearly every other case of ALS.[23] Abnormal aggregation TDP43 is a pathological feature present in most ALS cases (up to 97%) in which the protein that typically localizes to the nucleus for functioning in transcription becomes misfolded and aggregates in the cytosol.[25] The protein is ubiquitinated and hyperphosphorylated resulting in amyloid-like aggregation, increased hydrophobicity, and sequestration of essential cellular components.[25] These aggregates can be self-perpetuating operating in a prion-like mechanism.[4] Although, mutations to the gene encoding TDP43, TARDBP, accounts for about 4% of familial cases the neuropathological changes associated with TDP43 are found much more frequently on autopsy.[25] The fused in sarcoma (FUS) mutation shares functional homology with TDP-43 and accounts for 4% of familial cases.[26] Their shared pathology of misfolding and erroneous localization to the cytosol emphasize the importance of abnormal RNA metabolism in motor neuron degeneration.[23]

Other mutations linked to ALS have overlap with cases of Paget's disease such as optineurin mutations, valosin-containing protein, and sequestosome 1 mutations.[23,27] Mutations in ubiquitin 2 in both familial and sporadic cases implicate proteasome degradation of ubiquitinated proteins as a possible contributor to the pathology.[28] A large intronic hexanucleotide repeat expansion in C9ORF72 accounts for 40% of familial ALS cases and 7% of sporadic cases in people of European ancestry.[23] RNA foci are observed in patients with C9ORF72 which again implicates disruption of RNA metabolism through sequestration of RNA-

binding proteins and other RNA species.[29] On top of the plethora of implicated inherited mutations spontaneously occurring mutations have also been implicated in ALS.[23]

The similarities in genetic architectures between familial and sporadic ALS has led to the view that rigid dichotomizing of ALS into familial and sporadic disease is outdated and oversimplified.[4] Since the two types share many mechanisms of neurodegeneration including mitochondrial dysfunction, axonal transport, toxic protein aggregation, impaired protein degradation, prion-like spreading, excitotoxicity, oxidative stress, hypermetabolism, inflammation, and RNA metabolism defects.[30] This evidence indicates that ALS is a clinically and genetically heterogeneous neurodegenerative syndrome with multiple underlying pathophysiological mechanisms.[4]

Current Therapeutics for ALS

The complexity underlying ALS has led to a variety of attempted treatments, however, none have been able to reverse neural damage and cure the disease despite the fact that the syndrome was first described more than a century ago in 1869.[31] This does not mean that considerable effort has not been put towards finding a treatment. More than 60 molecules and 30 genes have been implicated in the pathogenesis of ALS.[17,23] These studies have led the discovery of for major of pathogenesis: excitotoxicity, inflammation, oxidative stress, and destruction of neurons.[31]

Excitotoxicity

The first avenue of clinical investigation was based on the hypothesis that aberrant glutamatergic system overactivation leads to death in motor neurons.[32] This lead to clinical trials and eventually the FDA approval of riluzole in 1995.[31] Riluzole's mechanism is highly complex and modulates the glutamate receptors indirectly by modifying the sodium channel current,

potentiation of calcium-dependent potassium current, and inhibition of neurotransmitter release.[33] Riluzole is estimated to be used by 50-75% of people with ALS.[34] However, riluzole only has modest benefits, prolonging life span by a mere 2 to 3 months.[33] In the United States, treatment with Riluzole costs about $10,000 USD per year and the cost effectiveness and quality of life of patients treated with Riluzole have not been assessed.[33]

Neuroinflammation

Numerous studies have investigated the immune system's role in the pathogenesis of ALS. One study found microglial activation at the site of motor neuron damage in ALS patients and found a positive relationship between the intensity of microglial activation and motor neuron degeneration.[35] An increase in the number of mast cells, another cell of the immune system, is associated with denervation of neuromuscular junctions and a feature consistently found in the muscles of ALS subjects.[25,36] Additionally, the presence of infiltrating monocytes and macrophages increases as ALS progresses in SOD1 mice.[35] Because neuroinflammation is a prominent pathological finding in ALS patients, eight compounds with primarily anti-inflammatory actions have been assessed in their treatment for ALS patients.[31] However, only one molecule has shown promise in late-stage clinical trials.[31] This molecule, named masitinib, is a highly selective tyrosine kinase inhibitor that has prolonged survival in SOD1 model mice through preventing CNS neuroinflammation.[31] In SOD1 mice, masitinib prevented mast cell and neutrophil infiltration, axonal pathology, and secondary-demyelination.[36] The addition of masitinib to riluzole treatment in a clinical trial slowed functional decline in ALS patients by 27%.[37] Masitinib is currently deemed an orphan drug by the FDA and, therefore, is not currently being used to treat ALS.[31]

Oxidative Stress

Excessive production of reactive oxygen species and resultant oxidative stress has been implicated in the pathogenesis of ALS and was first considered in the pathology due to the discovery of mutated superoxide dismutase 1 in one-fifth of ALS cases.[24,31] The finding of increased protein carbonyl levels in the spinal cord and motor cortex of patients with sporadic ALS, and increased 3-nitrotyrosine levels in SOD1 familial patients also implicate oxidative stress.[38] Additionally, oxidative stress causes TDP43 and FUS delocalization from the nucleus to the cytoplasm and increases both proteins tendency to aggregate.[39,40] One FDA approved drug currently is used to address oxidative stress in ALS patients: Edaravone. Edaravone is an intravenous free radical scavenger that has been proven to eliminate lipid peroxides and hydroxyl radicals that damage neuronal cells.[41,42] It also mitigates the dysfunction of the blood-brain barrier in rats.[42] Edaravone decreases oxidative stress as measured by a decrease in 3NT, a marker of oxidative stress. It has clinical significance for patients and leads to better scores on the ALSFRS-R, a measure specifically designed for the evaluation of functioning in ALS patients.[41,43] Edaravone was approved in the USA in May of 2017 and was the first FDA-approved treatment for ALS since the approval of riluzole in 1995.[44] However, it has not been shown to reverse neuronal damage.[44] Additionally, Edaravone has a rigorous treatment regimen requiring a cycle of two weeks of daily intravenous infusions followed by a period of two weeks drug-free.[31] Edaravone costs $145,500 USD per year cost before insurance and typically requires patients to have a port placement for intravenous administration, assistance with travel, and sufficient time to sit through the treatment.[44] These obstacles limit many patients from treatment and call for more accessible and effective treatments.

Neurodegeneration

Another avenue that many clinical trials have explored is the use of neurotrophic growth factors. Neurotrophic growth factors are active in neuron development, neural plasticity, neurogenesis, neural disease, and neural injury.[45] Since amyotrophic lateral sclerosis has such complex pathophysiology without a single causative mechanism, protection of the motoneuron with neurotrophic factors has emerged as a rational approach. The three factors that have been investigated in humans are brain-derived neurotrophic factor (BDNF), ciliary neurotrophic factor (CNTF) and insulin-like growth factors (IGF-1).[31] BDNF protects neurons against in vivo excitotoxicity, a key mechanism in ALS.[46] CNTF has direct neuroprotective effects on degenerating motoneurons in stress-induced conditions.[45,46] Whereas, IGF-1 is able to rescue motoneurons and reduce excitotoxicity.[45] However, these neurotrophic factors were all investigated from 1995-2008 and another neurotrophic factor clinical trial has not occurred since.[31] Importantly, the neurotrophic factors have been studied using various modes of delivery such as subcutaneous delivery and intrathecal administration but not through the use of drug-loaded nanofibers.[45] It is likely that poor dosage, ineffective delivery, and poor translation from mouse models could all be possible contributors to the failures of clinical trials involving neurotrophic factors.[45] Therefore, a new drug delivery system that maintains consistent levels of drug at appropriately high doses needs to be developed and examined to determine if the promising effects of neurotrophic growth factors, current FDA approved drugs, and novel drugs can be improved upon in meaningful ways for ALS patients.

<u>Alginate Nanoscaffolds</u>

To mitigate problems with drug delivery and to address multiple of the identified disease mechanisms of amyotrophic lateral sclerosis, the current study focuses on developing and

optimizing a cross-linked alginate nanoscaffold for the effective delivery of drugs to amyotrophic lateral sclerosis affected motor neurons. Alginate was chosen as the primary material for the construction of this novel nanofiber scaffold because of its biocompatibility, low toxicity, relatively low cost, and the ability to be altered through relatively simple modifications.[47] Additionally, alginate has a range of bioactivities such as anti-tumor properties, counteraction of oxidation, regulation of immune responses, reduction of inflammation, and neuroprotection.[47]

Producing the scaffold on a nanoscale was chosen because many biological scaffolds present in the natural extracellular matrix in human tissue are on the nanoscale, therefore, this scale provides the highest similarity to natural systems.[47] The nanoscale was also chosen because it allows for a large surface area per volume ratio and a very short diffusion distance for loaded drugs.[48]

Alginate is a naturally occurring anionic polymer that is obtained from brown seaweed.[49] It is typically extracted from brown algae (Phaeophyceae), but other sources are utilized such as alginate producing bacterium.[49] Polymeric nanofibers of alginate are of particular interest in regenerative medicine because they can be tailored to mimic the extracellular matrix in terms of structure, chemical composition, and mechanical properties.[50] Alginate nanofibers bear resemblance to glycosaminoglycan, an abundant proteoglycan found in the extracellular matrix of humans, and can be used to provide similar mechanical support and to regulate cellular activities.[50] The composition of the alginate varies depending on the natural source with differing ratios of its two sterically different repeating units: (1→4)-a-L-guluronate (G unit) and (1→4)-b-D-mannuronate (M unit).[50] These subunits are linked by β-1,4-glycosidic bonds.[47] Only the guluronate blocks are believed to participate in intermolecular cross-linking with divalent cations

in a manner termed the egg-box model shown in Figure 1.[49] Therefore, the composition sequence, G-block length, and molecular weight are all highly influential factors affecting the physical properties of alginate scaffolds.[49]

Manipulation of molecular weight changes the physical properties of alginate fibers with higher molecular weight leading to greater mechanical strength due to increased cross-linking.[49] However, higher molecular weight also leads to low bioavailability.[49] To circumvent this pitfall, degradation of alginate into oligosaccharides is utilized to increase the absorption of drugs and encourage biocompatibility.[47] Additionally, alginate is often partially oxidized with sodium periodate to increase bioavailability, with the degree of oxidation strongly influencing the degradation of the fibers.[49] A partially oxidized oligomer of alginate is shown in Figure 2.

Cross-linking alginate can also increase biodegradability by the release of divalent ions and subsequent incorporation of monovalent cations present in the biological systems such as sodium.[49] Ionic cross-linking is the most common method used for alginate cross-linking.[49] The amount of cross-linking with alginate depends on the charge density of the ion and the number of guluronate blocks.[49] Therefore, in this study oxidized oligosaccharides of alginate cross-linked to strontium, barium, and calcium were evaluated for their differences in drug release profiles and their ability to biodegrade.

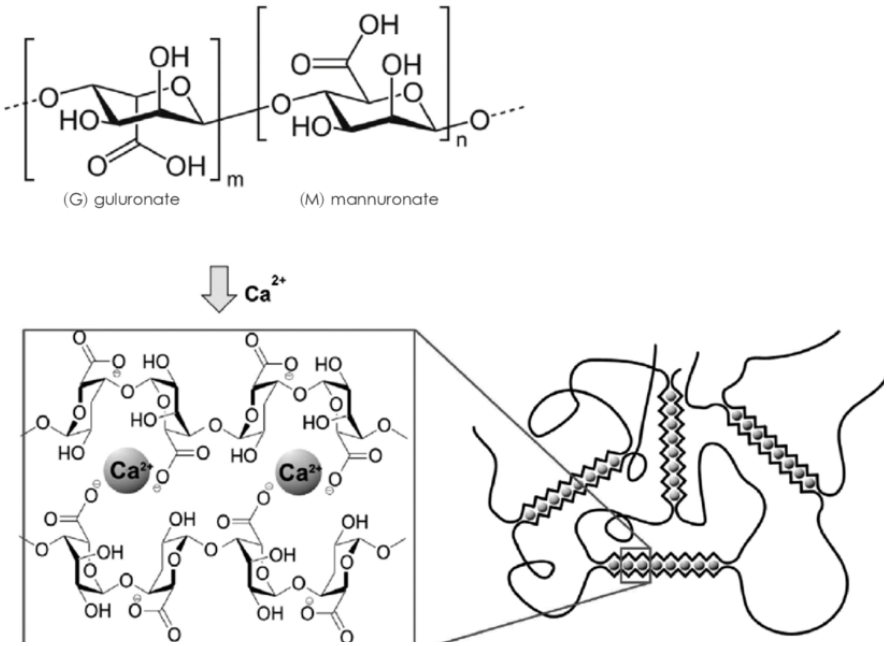

Figure 1: Schematic representation of the monomeric units of alginate (guluronate and mannuronate) and their interaction in an egg-box manner with the divalent calcium ion.[49]

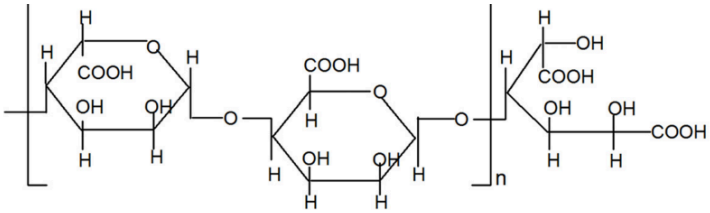

Figure 2: Schematic representation of chemical structures of alginate-derived oligosaccharide prepared by oxidative degradation.[51]

The biological effects of alginate alone make it an attractive biomaterial for the treatment of amyotrophic lateral sclerosis. It possesses antioxidant activity, immunoregulatory activity, anti-inflammatory activity, and neuroprotective activity.[47] All of which would be great utilities for mitigating the multi-faceted pathogenesis of amyotrophic lateral sclerosis which involves reactive oxygen species, neuroinflammation, dysregulation of cells of the immune system, and neurodegeneration.[31,36] Several studies have documented alginate's ability to inhibit oxidative stress-induced neurotoxicity in *in vitro* Alzheimer's rat models as well as its ability to inhibit the formation of amyloid β.[52] Alginate has also been implicated in immunoregulation through

induction of cytokine activity.[53] Additionally, multiple studies have demonstrated alginate's ability to activate macrophages and the host immune system.[53,54] With its ability to influence the host's immune system, alginate has subsequently been shown to suppress neuroinflammation by suppressing the activation of microglia and attenuating the production of inflammatory mediators.[51] Alginate's neuroprotective activity stems from its ability to inhibit oxidative stress and regulate the immune system, however, alginate is also an antiglycation agent.[47] Advanced glycation end-products (AGEs) participate in the pathogenesis of neurodegenerative disorders and are associated with abnormal brain protein cross-linking, oxidative stress, and neuronal loss.[47] These biological properties make it ideal to couple with a dynamic drug delivery system, in fact, alginate nanofibers have been investigated for their ability to deliver a variety of drugs.

Alginate Nanoscaffold Release Kinetics

The versatility of alginate oligosaccharide derivates can be exploited to regulate the kinetics of drug release.[49] Alginate nanofibers are nanoporous.[49] The nanopores allow for rapid diffusion of small molecules that can be altered as a function of amount of oxidization and cross-linking. The goal of elucidating the release kinetics of varying alginate nanofibers to determine if they can maintain the drug level in the target tissue within the therapeutic window, above the minimum effective concentration and below the minimum toxic concentration, without the need for multiple doses.[48] Often single large doses exceed the minimum toxic concentration but rapidly fall below the minimum effective concentration, therefore, a sustained release within the range is desirable.[48] Providing the drug in one dose avoids fluctuations of drug concentration, reduces risk to the patient for repeated invasive delivery mechanisms, and avoids non-compliance issues from the patient. Because sustained release at a low dosing frequency is desired zero-order drug release profiles (continuous release) are often pursued.[48]

As a biodegradable polymer alginate's drug release occurs via three mechanisms: diffusion-controlled release, solvent-controlled release, and degradation-controlled release. Cross-linked alginate nanofibers incorporate drugs into its polymer matrix and the drug release is partially driven by the concentration differential across the membrane.[50] Additionally, solvent transport into the drug carrier can displace the cross-linked cations used in alginate and initiate drug release.[50] Water can also diffuse into the system resulting in the swelling of polymer followed by drug release.[55] The release rate is determined by the relaxation rate of the polymers, the relaxation rate, in turn, relies on the amount of cross-linking.[48]

Finally, degradation of the nanofiber also plays a role in the release kinetics. Although alginate is inherently non-degradable in mammals due to lack of the enzyme alginase, surface erosion and destruction of cross-linking structure degrade the polymer in biofluids.[49] In nanofibers, the polymer degradation occurs faster because of the short distance water must travel to reach the interior of the fiber.[48] Degradable polymeric systems are preferable because they can be readily removed from the body without causing harm. In fact, alginate oligosaccharides have the ability to be cleared by the kidney.[56] The combination of these release types can then be evaluated concomitantly to determine if the release mechanism is Fickian or non-Fickian diffusion using the semi-empirical Peppas model illustrated in equation 1, where M_t is the cumulative amount of drug released at time t, M_∞ is the cumulative amount of drug released at time ∞, k is a constant, and n is the order of the release. All of these values can be determined experimentally.[48] Again, with zero-order release kinetics as the most favorable release profile for drug delivery.

$$\frac{M_t}{M_\infty} = kt^n \quad (1)$$

Alginate's Current Applications

Alginate has an extensive track record for biologically meaningful drug release in a variety of applications due to its adaptability and demonstrated benefits. Various alginate technologies have been applied for the regeneration of various tissues and been successful in the regeneration of blood vessels, bone, cartilage, muscles, nerves, pancreas, and liver.[49,57,58] Vascular endothelial growth factor (VEGF) and basic fibroblast growth factor (bFGF) have a sustained and localized release from alginate fibers in applications related to increasing neovascularization in ischemic tissue.[49] Alginate cross-linked with calcium has been used to sustain release of dibutyryl cyclic adenosine monophosphate and stromal cell-derived factor 1 in for wound healing.[57]

Alginate has also demonstrated effective delivery of bone morphogenetic proteins (BMPs) to enhance osteogenic differentiation of bone-marrow derived cells in vitro.[59] Sustained release of hepatocyte growth factor and fibroblast growth factor from alginate gels have enhanced long-term survival and outward migration of primary myoblasts in damaged muscle tissue and have supported extensive repopulation of host muscle tissues at the wound sites.[58] With the promising effects of alginate nanofibers on other tissues of the body, research has extended into the ability of alginate fibers to assist in the repair of the central and peripheral nervous systems. Alginate fibers incorporated into acute cervical spinal cord lesions in rats directed axonal growth, whereas, alginate gels were able to serve as a scaffold to restore a 50-mm gap in cat sciatic nerves while promoting outgrowth of regenerated axons.[60,61] Alginate nanofibers have also been evaluated in the context of their ability to fill up surgical residual cavities and were found to provide structural support and promote neural tissue reconstruction.[62]

Methylene Blue

With the many successes of alginate biomaterials in tissue regeneration, and specifically their ability to act as a scaffold for neuron and axonal regeneration, this study focuses on analyzing various configurations of alginate nanofibers cross-linked with different cations. The properties of the nanofibers that were focused on were the loading efficiencies with the drug methylene blue, the release profiles, and degradation times. Methylene blue, the first synthetic drug, is a tricyclic phenothiazine.[63] Under physiological conditions, methylene blue is a cation which makes it favorable for interaction with the anionic alginate nanofibers. Additionally, an extensive amount of literature has been published on methylene blue's usefulness in treating a plethora of diseases including depression, enzymopenic hereditary methemoglobinemia, Ifosfamid-induced neurotoxicity, vasoplegic adrenaline resistant shock, and Alzheimer's disease.[63]

Particularly, methylene blue was chosen because it has been evaluated for its ability to slow down neurodegenerative diseases. Methylene blue has been found to inhibit the aggregation of tau protein and of Aβ peptides in the low μmol/L range; both of which are common in Alzheimer's disease.[64,65] However, what is most interesting is methylene blue has aggregation inhibitory potential for the protein TDP43, a protein that is aggregated in up to 97% of all amyotrophic lateral sclerosis patients.[25,66] It is unclear whether the therapeutic use of methylene blue for neurodegenerative diseases is due to its aggregation inhibitory effect or the antioxidant activity by interaction with the electron transport chain, however, its positive effects remain relatively consistent.[63] Additionally, behavioral and memory studies with rats have shown improvement without side effects for low doses of methylene blue.[67] These positive effects of

methylene blue are assumed to be due to improved oxygen utilization via stimulation of mitochondrial cytochrome c oxidase.[67]

Methylene blue is very inexpensive, can permeate the blood-brain barrier irrespective of the route of administration, and has approximately 73% bioavailability.[68,69] Along with these properties and its potential prevention of TDP43 protein build up methylene blue was chosen as the model drug in the pre-clinical testing phases for this study. Methylene blue shares structural and dimensional similarities with the current FDA approved drugs for the treatment of amyotrophic lateral sclerosis. Their structural comparison can be seen in Figure 3. Therefore, it is ideal to use the much cheaper drug as a model for the characterization and development phase of alginate nanofibers so that the optimal nanofibers can then be applied and evaluated *in vivo* and *in vitro* with FDA approved drugs and methylene blue at a later time.

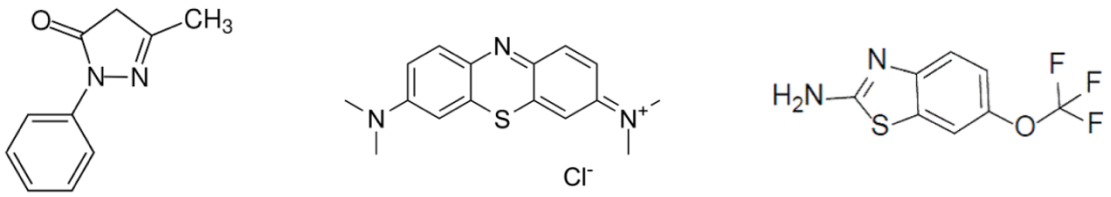

Edaravone Methylene Blue Riluzole

Figure 3: Chemical Structures of Edaravone, methylene blue, and Riluzole, respectively.

The goal of this study is to synthesize and characterize alginate cross-linked nanofibers in their release of methylene blue. For that reason, no specific hypotheses were made about the ability of each type of nanofiber to load and release methylene blue. However, it was hypothesized that higher concentrations of cross-linking solution would lead to the synthesis of more robust nanofibers with longer degradation times.

Methods

Materials

An immersive rotary jet spinning system similar to the apparatus depicted in Figure 4 was used to synthesize the alginate nanofibers.[70] The immersive rotary jet spinning system was built with the following parts: a 250-watt DC motor with variable speeds from 1000 to 80,000 RPM, a motor control board, a microcontroller, and a potentiometer. Changing the resistance of the potentiometer changed the voltages supplied to the motor. The rotating reservoir was manufactured from polysulfone and included one 175 μm diameter orifice. The speed of the rotating reservoir ranged from 15,000 to 65,000 RPM, while the collector reservoir spun at 350 RPM. The reservoir for the precipitating bath was a 500 mL beaker on a stir plate with variable power to drive a stir bar. The precipitating bath used was a miscible liquid to the solution solvent but did not have the ability to solubilize the polymer. In this case, it was the varying cation chloride solutions, $BaCl_2$, $SrCl_2$, and $CaCl_2$. The gap distance between the precipitating bath and the extrusion orifice, termed the air gap distance, was controlled independently by changing the height of the reservoir relative to the precipitating solution vortex. Lyovapor™ L-200 Classic was used to lyophilize the samples. All samples were placed in 30 mg aliquots in VWR Glass vials with phenolic caps for further analysis.

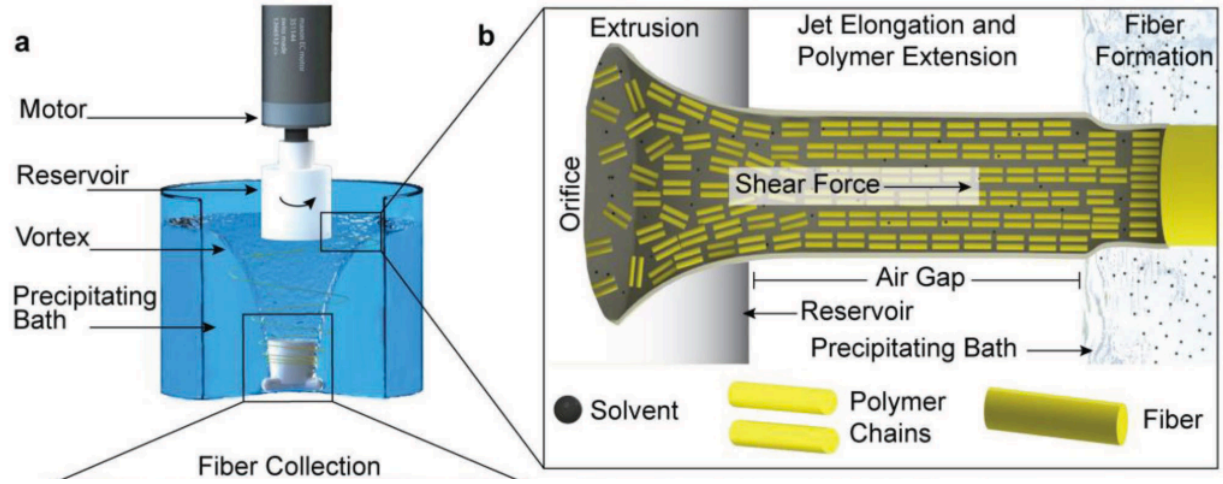

Figure 4: the immersion rotary jet-spinning system spins a nanofiber through an orifice of a rotating reservoir (a). In the air gap (b), the polymer solution undergoes jet elongation and thinning while the polymer chains align. After the jet elongation the polymer solution enters the cross-linking bath to form nanofibers. The vortex pull and collect the fibers in the precipitating bath.[70]

VWR Scientific Sheldon Lab 1350FM Forced Air Oven Mint/ 240C/4 CuFt /4 Mo was used to maintain the samples at a constant temperature. A VWR Hot Plate Mini Reciprocal Shaker placed inside of the oven (Speed: 20 - 240 osc/min, Stroke: 1 in, Maximum Capacity: 40 lbs, Controls: Digital, Bodine DC motor which drives the platform through a filtered SCR controller, Electrical: 230Vat 50/60hz, Dimensions: 16.5 x 11 x 10 in) was used to load the fibers with methylene blue under constant agitation. After the drug loading period, supernatant samples were analyzed with the Hitachi Photodiode Array Bio-spectrophotometer U-0080D (WL mode: 1WL, wavelength: 663 nm, path length: 10 nm, integration: 32, High (abs): 1, low (abs): 1, high (nm): 800, low (nm): 500). The Hitachi High-Technologies Corporation 2003 Program No. 7A00618-02 was used to analyze data.

A low-power scanning electron microscope Tescan Vega II was used for confirmation of nanostructures. Additionally, a low-power x-ray powder diffraction Rigaku miniflex was used

for the routine check of known lattice-structures. An optical microscope Olympus BX51 was used to check samples before scanning electron microscopy.

Required chemicals include sodium alginate (CAS: 9005-38-3, Sigma-Aldrich, St. Louis, MO), methylene blue solution 1% aqueous (CAS: 61-73-4, Ward's Science St Catharines, ON, Canada), strontium chloride, anhydrous 95% powder (Beantown Chemical, Hudson, NH), calcium chloride, anhydrous 97% beads/powder (Beantown Chemical, Hudson, NH), and barium chloride dihydrate 99+% (Alfa Aesar, Heysham, LA3 2XY, England). Additionally, PBS tablets 100 mL (VWR Chemicals, Solon, Ohio) with the composition of 137 mM sodium chloride, 2.7 mM potassium chloride, and 10 mM phosphate buffer were utilized.

Alginate Nanofiber Synthesis

Sodium alginate (Sigma-Aldrich St. Louis, USA) solutions of 1% weight/volume were made in 400 mL of deionized water and were heated with constant agitation for 1 hour. The crosslinking agents, strontium, barium, and calcium were prepared from $SrCl_2$, $BaCl_2$, and $CaCl_2$ at the following concentrations: 50 mM, 100 mM, 200 mM, 300 mM, and 400 mM. The varying concentrations were used to evaluate the mechanical integrity of the nanofibers relative to the degree of crosslinking as well as to examine the differing release profiles as the crosslinking agent changed in identity and in concentration. These precursor solutions were then used to obtain alginate nanofibers in which alginate solution was extruded from a reservoir into the crosslinking bath under a vortex created by immersive rotary jet spin, a centrifugal dry jet wet spinning platform. The synthesized alginate nanofiber scaffolds were then lyophilized below their glass transition temperature. Lyophilization has three primary stages: freezing phase, sublimation phase, and adsorption phase. The fibers are brought to temperatures below the triple point, then the pressure is lowered, and heat is added to the material so water will sublimate, then

ionically bound water molecules are removed by raising the temperature above that used in the sublimation phase. Lyophilization reduces drying times by 30% and can dry the nanofibers to 1-5% residual moisture. The morphological properties of the nanofibers were assessed via scanning electron microscopy (SEM). The goal was to synthesize novel bioscaffolds as effective and neuroprotective agents with the desired pore structures and surface chemistry.

Methylene Blue Loading and Release Studies

Methylene blue (methylthioninium chloride) was loaded to the fibers at various loading concentrations to determine the optimum dose. Loading concentrations that were assessed were 12.2 nM, 48.8 nM, 97.5 nM. The methylene blue solutions were made with 1x phosphate-buffered saline (PBS) to simulate the ionic environment of extracellular fluid. Phosphate buffered saline is commonly used in biological research and is a solution containing disodium hydrogen phosphate and sodium chloride. This solution helps to maintain a constant pH with osmolarity and ion concentration matching those of the human body (isotonic). The phosphate-buffered solution was made using PBS tablets to minimize variation that comes with measuring the compounds with analytical balances. Approximately 30 milligrams of cross-linked alginate nanofibers were placed in the chosen loading concentration for 18 hours. During this time the samples were protected from light, maintained at 37^{o}C, and were under constant agitation. These conditions were chosen to model extracellular conditions of the human nervous system which is maintained at similar conditions. Following the sample loading period, the samples were removed from the initial loading solution and washed twice with phosphate-buffered solution to mitigate the release of methylene blue and wash off weakly bound methylene blue. The methylene blue infused alginate nanofiber scaffolds were then ready for release studies.

The methylene blue infused alginate nanofiber scaffolds were transferred using clean tweezers to 3 mL of fresh phosphate-buffered solution. The solution was then placed in the forced air oven where they were maintained at 37°C, protected from light, and were under constant agitation. At the same time, the loading solution was then analyzed using ultraviolet spectroscopy at 665 nm. Methylene blue has a maximum absorbance at 665 nm. This was determined before the beginning of release studies so that the absorbance value could serve as a proxy for the concentration of methylene blue in various solutions.

To analyze the release profile of the methylene blue infused alginate nanofiber scaffolds, 1.5 mL aliquots of the phosphate buffered solution containing the methylene blue infused alginate nanofiber were extracted at pre-determined time intervals (30, 60, 90, 120, 150, 180 mins) using a micropipette. Once the aliquot was extracted for ultraviolet spectroscopy analysis, the same volume of 1x phosphate-buffered solution, 1.5 mL, was replaced to maintain the sample at a constant volume. The sample was then placed back into the oven to maintain the temperature at 37°C, protect it from light, and continue the agitation. Each nanofiber was analyzed in triplicate.

Data Analysis

Molarity information about each of the sample aliquots will be obtained via calibration curve extrapolation. All data are represented in graphs as the mean ±S.E.M (Standard Error Mean).

Results

Fourteen different configurations of alginate nanofibers were evaluated for their loading efficiency, release profiles, and degradation profile and are listed in Table 1. Selected fibers were analyzed with varying concentrations of methylene blue loading solutions. These solutions either consisted of 7.8 µL, 31.2 µL, or 62.4 µL of methylene blue in 20 mL of phosphate-buffered solution resulting in 12.2 nM, 48.8 nM, 97.5 nM methylene blue solutions, respectively. All nanofibers were analyzed morphologically with scanning electron microscopy to confirm the nanoporous and amorphous structure. A resulting micrograph of 200 mM strontium alginate is shown in Figure 5. Further macroscopic differences in fibers can be observed in methylene blue solutions in Figures 17-20 in the appendix.

Table 1: Summary of evaluated alginate nanofibers. The left column represents the cross-linking cation and the top row represents the cross-linking cation's concentration. The overlapping columns represent the loading concentration of methylene blue used for the nanofiber.

	Cross-linking concentration			
Cation	50 mM	200 mM	300 mM	400 mM
Strontium	31.2 µL	7.8 µL, 31.2 µL, 62.4 µL	31.2 µL, 62.4 µL	
Barium	31.2 µL	7.8 µL, 62.4 µL	31.2 µL	31.2 µL
Calcium		31.2 µL	31.2 µL, 62.4 µL	

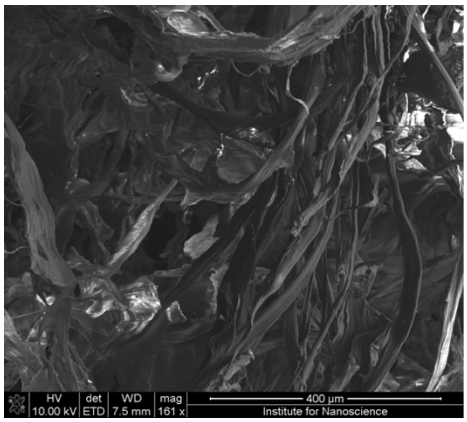

Figure 5: scanning electron microscope (SEM) image of 200 mM strontium alginate nanofibers.

The total loading efficiency of each nanofiber at varying loading concentrations was assessed via UV-Vis spectroscopy and calibration curve extrapolation. The nanofibers listed in Table 1 with their respective loading concentrations were analyzed. The total loading efficiency of the varying alginate nanofibers is of interest to minimize the amount of wasted loading drug and to determine which fiber effectively loads the greatest proportion of loading drug. The total loading efficiency of strontium alginate nanofibers peaked at 59.8% for 300 mM strontium cross-linked nanofibers at 31.2 µL loading concentration. All other strontium alginate nanofibers maintained a loading concentration efficiency between 17% and 26% and were not significantly different from one another. The loading efficiency of strontium alginate nanofibers is depicted graphically in Figure 6, as well as the loading efficiency of barium and calcium alginate nanofibers. The barium alginate nanofibers also had the largest loading efficiency when the cross-linking solution was 300 mM and the loading solution contained 31.2 µL. The loading efficiency for that fiber was 35.2%, significantly lower than its strontium counterpart. However, it did not differ significantly from the loading efficiency of the 200 mM barium alginate nanofiber and both of these fibers had improved loading efficiency from the 400 mM barium alginate nanofiber. Of the three calcium alginate nanofiber configurations, the two with maximum loading efficiency were not significantly different from one another (calcium 200 mM

@ 31.2µL, 24.9%; calcium 300 mM @ 31.2µL, 22.6%). However, they both had greater loading efficiency than the 300 mM calcium @ 62.4µL (9.37%). These results are depicted in Figure 6.

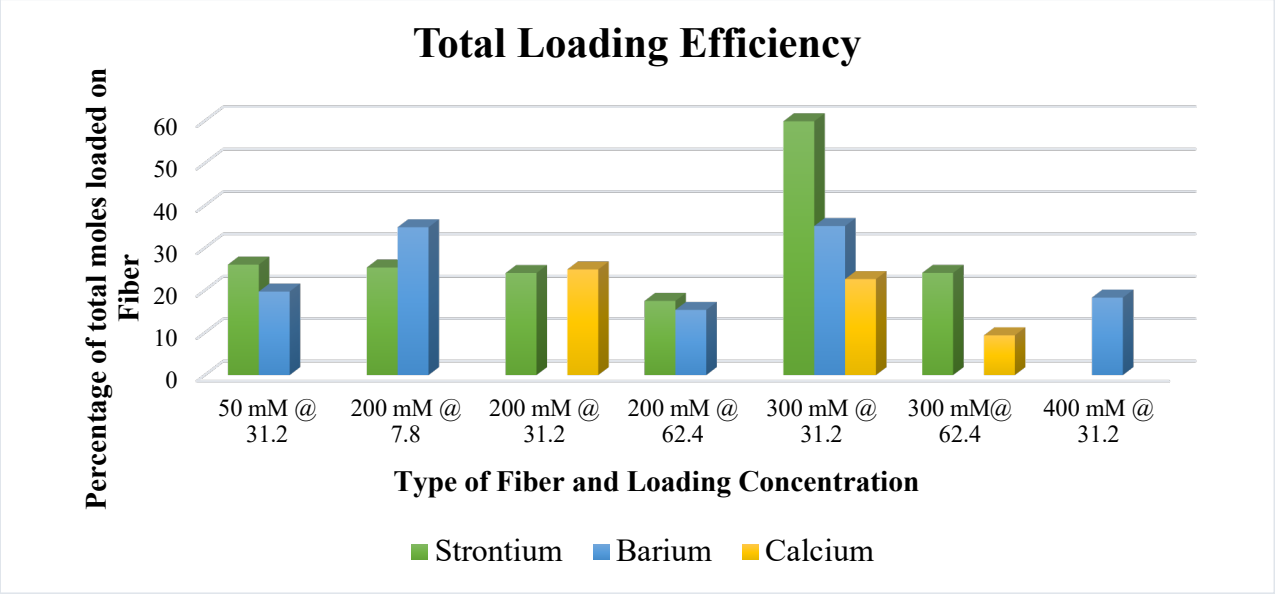

Figure 6: Total loading efficiency of Strontium, Barium, and Calcium cross-linked alginate nanofibers expressed as the percentage of loading methylene blue moles loaded onto the fiber after a 12-hour incubation period

To further standardize the analysis of the triplicate samples of each of the 14 nanofiber configurations, the nanofibers were analyzed for their loading efficiency per milligram of nanofiber. For the most part, the trends persisted that were described for total loading efficiency but were further differentiated from one another. The major change when analyzing on the milligram level was the loading efficiency of barium 200 mM @ 7.8µL. When standardizing by milligram this fiber conformed to the trend of lower loading efficiency than its strontium counterpart. The data depicting the percentage of total moles of methylene blue loaded per mg of fiber is shown in Figure 7.

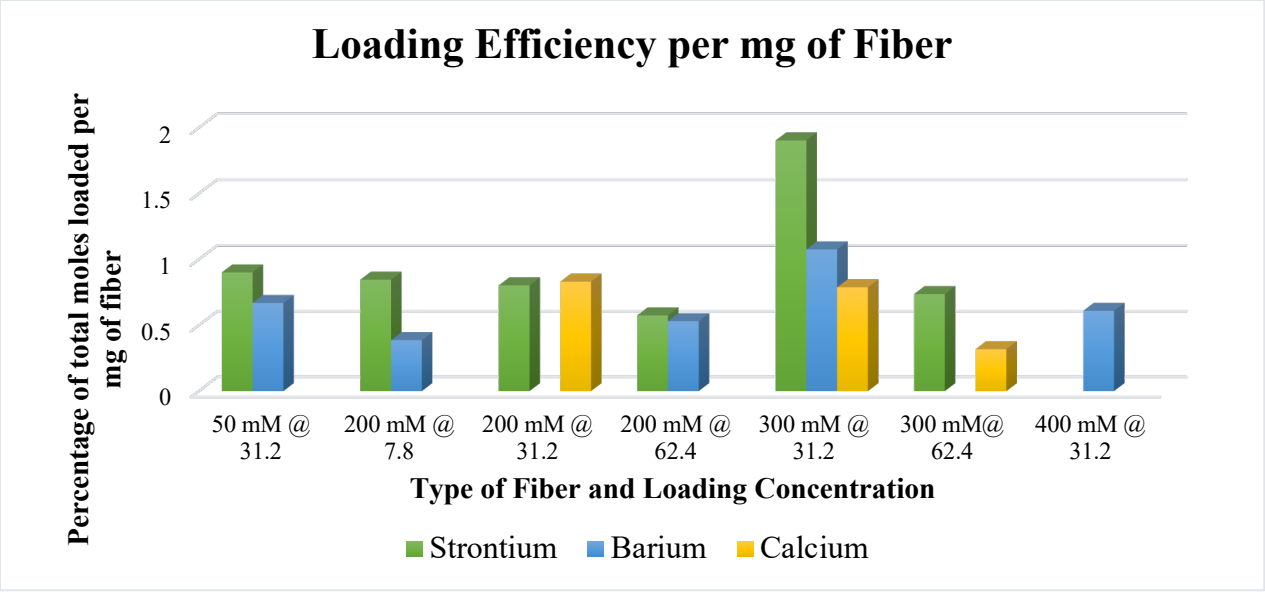

Figure 7: Loading efficiency of a mg of strontium, barium, and calcium cross-linked alginate nanofibers expressed as the percentage of total methylene blue moles loaded onto a milligram of fiber in a 12 hour incubation period

To analyze the effective dose that could be loaded onto each type of nanofiber the moles of methylene blue loaded onto each milligram of nanofiber were analyzed. This information is important to ensure proper dosing of the target drug when applied *in vivo*. The maximum number of moles loaded per milligram of nanofiber was observed for strontium 300 mM @ 31.2µL with the ability to load about 2.79 nanomoles per milligram of nanofiber. When strontium alginate nanofibers were significantly different from their counterparts, they consistently outperformed their barium and calcium counterparts for ability to load the most moles. Barium nanofibers loaded the most moles in two conditions: 200 mM @ 62.4µL and 300 mM @ 31.2 µL with the ability to load about 1.5 nanomoles per mg of fiber. The trends in the number of nanomoles loaded are depicted in Figure 8.

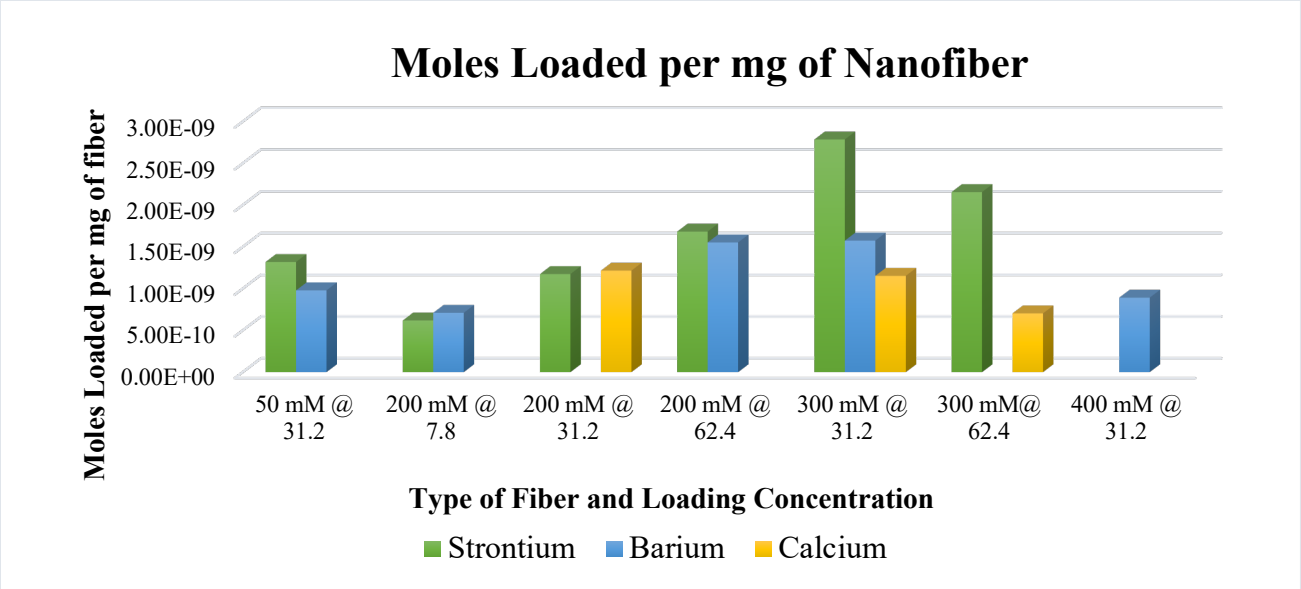

Figure 8: The loading moles capacity of strontium, barium, and calcium cross-linked alginate nanofibers expressed as the amount of methylene blue moles loaded on a milligram of nanofiber in a 12-hour incubation period

The release profiles of the strontium, barium, and calcium alginate nanofibers were analyzed to determine the percentage of loaded drug released at 30-minute time intervals. The release profile is informative for determining if the fiber releases drug concentrations above the minimal toxic dose or if it consistently releases below the minimal effective dose. The goal for release is a consistent zero-order release profile that maintains drug concentrations between the minimal toxic dose and above the minimal effective dose. Two fibers of strontium alginate nanofibers, 200 mM @ 7.8µL and Sr 200 mM @ 62.4µL, showed rapid release profiles followed by degradation. Whereas, three strontium alginate nanofibers, Sr 200 mM @ 7.8µL, Sr 300 mM @ 31.2µL, and Sr 300 mM @ 62.4µL, had non-significantly different release profiles. These fibers showed slow release with a flattening after the release of 20.2-28.6% of all loaded methylene blue. Sr 300 mM @ 31.2µL nanofibers had very different release profile than the others resulting in the cumulative release of 78% of all loaded methylene blue. These trends are represented in Figure 9.

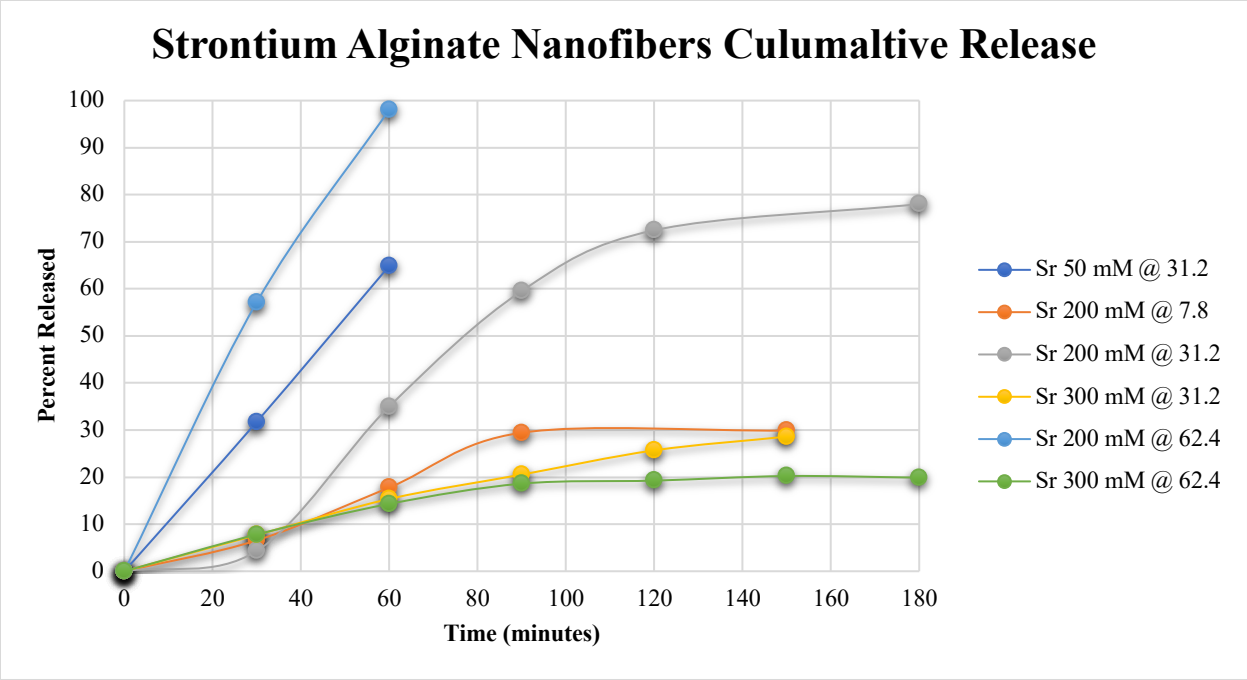

Figure 9: Methylene blue release profile for various strontium cross-linked alginate nanofibers, represented by the percentage of loading methylene blue moles released at various time points. Data stopping before the 180-minute mark represent the degradation of the nanofiber.

Barium alginate nanofibers were also examined for their release profile until degradation. Barium 200 mM @ 7.8, barium 300 mM @ 31.2µL, and barium 400 mM @ 31.2 µL were not significantly different in their release profiles. Whereas barium 200 mM @ 62.4 µL showed the most prolonged and steady release of all the barium nanofibers. The barium 50 mM @ 31.2µL released methylene blue quickly as well as quickly degraded. The barium alginate nanofibers release profiles are depicted in Figure 10. Whereas, the release profiles of the three calcium alginate nanofibers are depicted in Figure 11. The two 300 mM calcium alginate nanofibers show very different release profiles; however, the 200 mM calcium alginate nanofiber is not significantly different from the 300 mM @ 31.2 µL nanofiber.

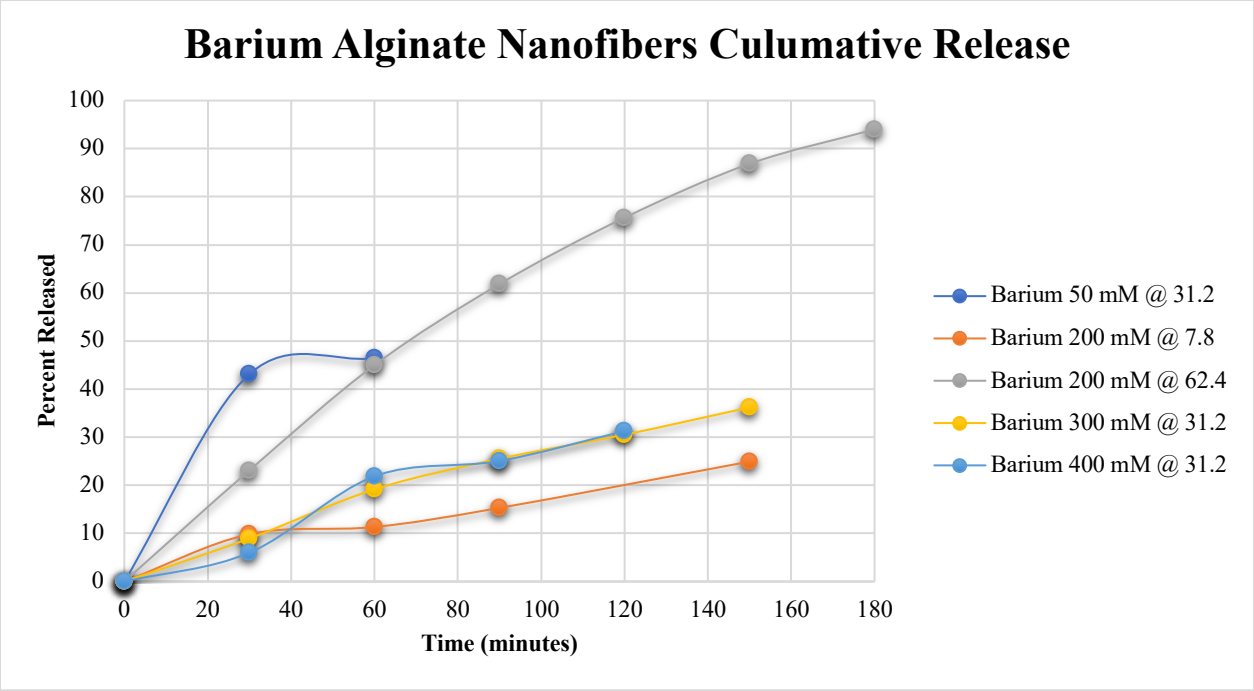

Figure 10: Methylene blue release profile for various barium cross-linked alginate nanofibers, represented by the percentage of loading methylene blue moles released at various time points. Data stopping before the 180-minute mark represent the degradation of the nanofiber.

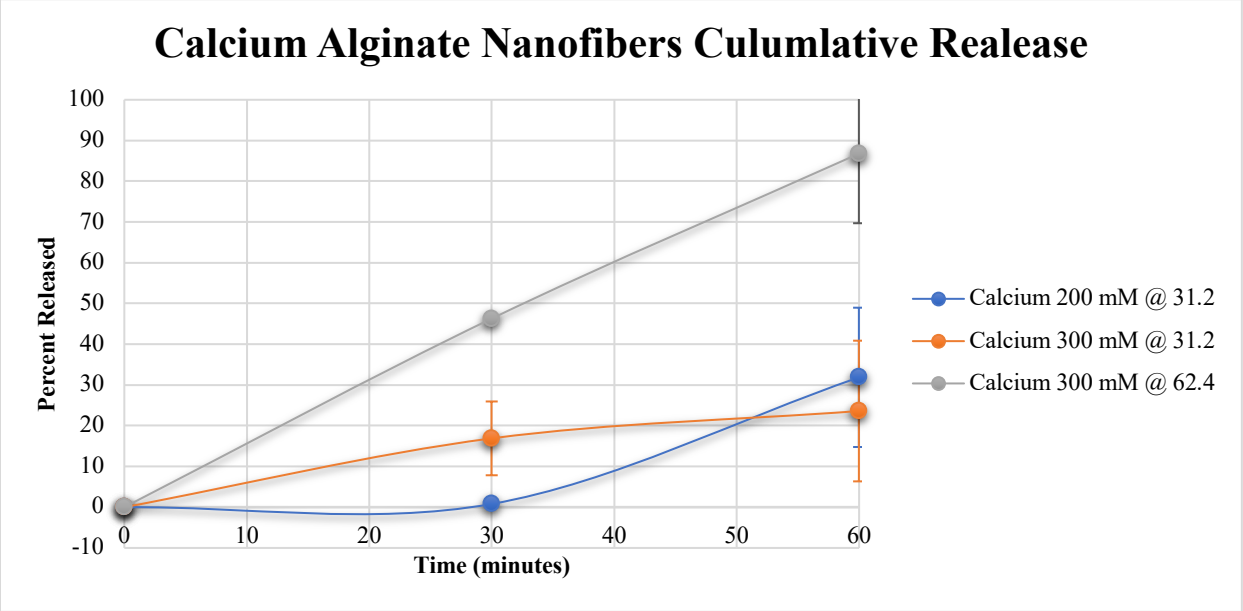

Figure 11: Methylene blue release profile for various calcium cross-linked alginate nanofibers, represented by the percentage of loading methylene blue moles released at various time points. Data stopping before the 180-minute mark represent the degradation of the nanofiber.

To further standardize the comparison between fibers of the same type, the percent of total methylene blue moles loaded onto the fiber released was analyzed per milligram of nanofiber. This standardization reduced the differences observed in the strontium alginate nanofibers, however, the Sr 300 mM @ 31.2 µL and Sr 200 mM @ 62.4 µL remained significantly different from the other four fibers. This trend can be observed in Figure 12. With Sr 300 mM @ 31.2µL resulting in the most prolonged release and released the highest percentage of loaded moles into the surrounding solution and the Sr 300 mM @ 31.2µL resulting in a shorter release with less of the total moles released at the end of the study.

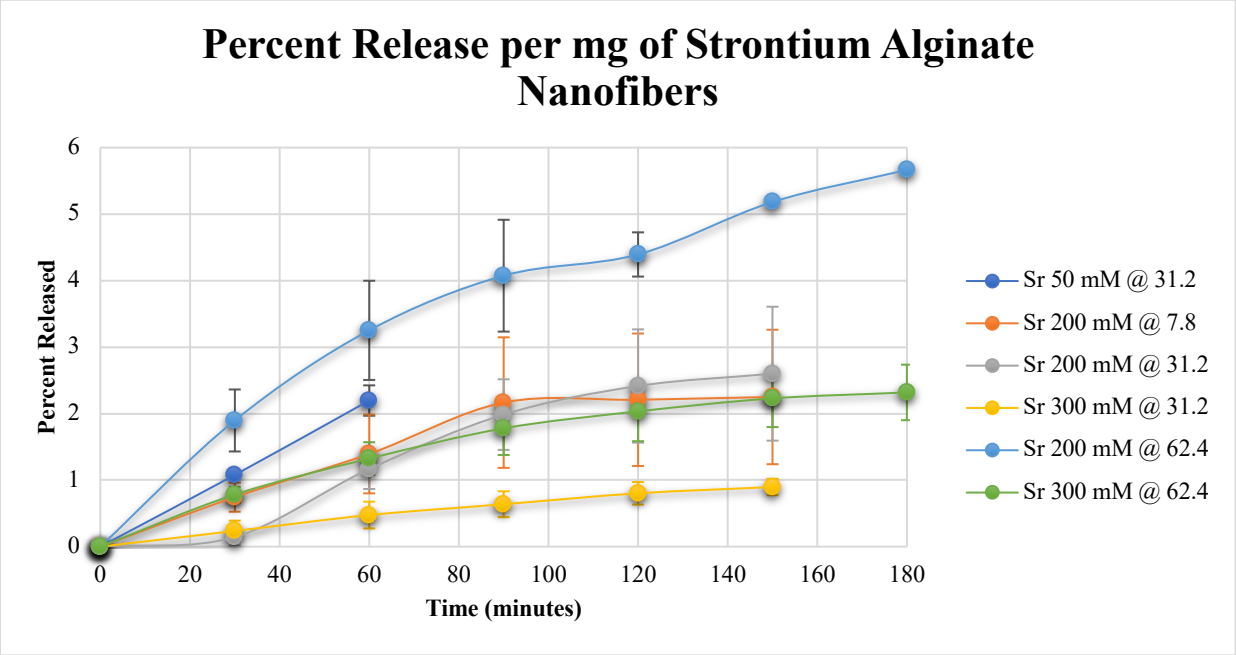

Figure 12: Methylene blue release profile of strontium cross-linked alginate nanofibers represented by the percent of total moles loaded onto the nanofibers release at various time points. Data stopping before the 180-minute mark represent nanofibers that degraded.

The standardization to milligrams also produced a reduction in the difference among the barium alginate nanofibers as depicted in Figure 13. However, barium 200 mM @ 62.4 µL and barium 50 mM @ 31.2 µL continued to have the highest percent release that was significantly different from the other three fibers.

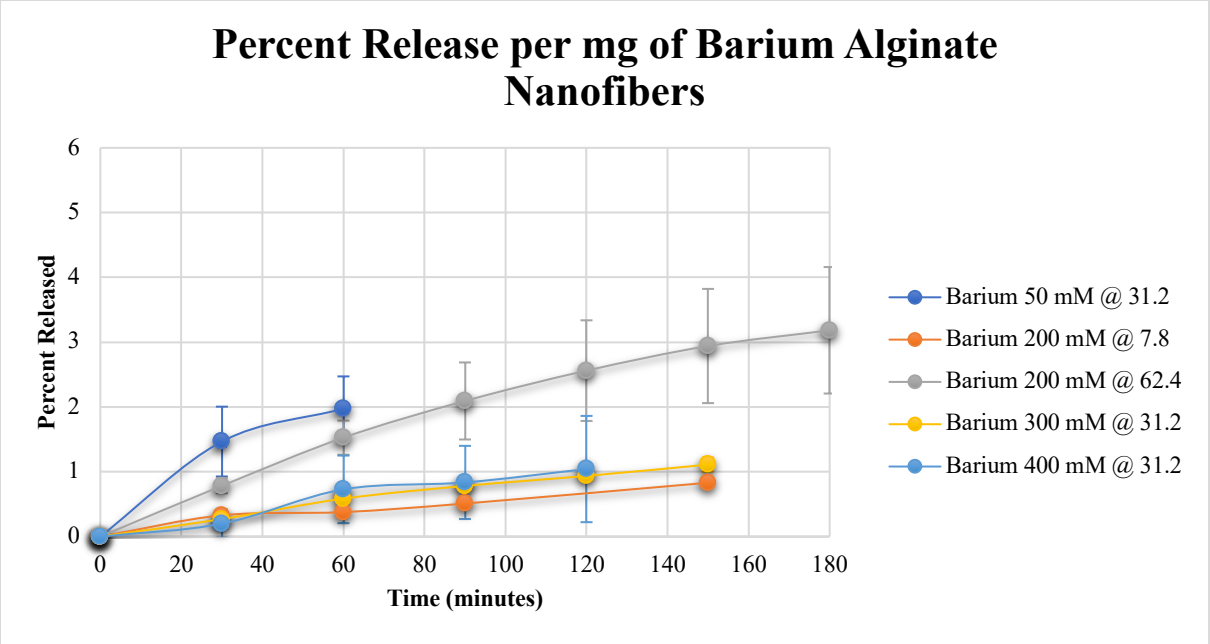

Figure 13: Methylene blue release profile of barium cross-linked alginate nanofibers represented by the percent of total moles loaded onto the nanofibers release at various time points. Data stopping before the 180-minute mark represent nanofibers that degraded.

The calcium alginate nanofiber 300 mM @ 62.4 µL remained significantly different from the other two calcium alginate nanofibers when evaluated at the milligram level. The calcium alginate nanofiber trends are depicted in Figure 14.

The average degradation times of the nanofibers were also analyzed. Their degradation is an essential factor in their utility; however, it is optimal that the fibers do not degrade before 100 percent of the loaded drug is released. Only the strontium 200 mM @ 62.4 µL nanofiber released 100% of its loaded concentration before degradation and it did so rapidly. No other fiber achieved this. The trend in degradation time is depicted in Figure 15. Barium alginate nanofibers consistently took longer to degrade than the strontium alginate nanofibers except in the case of 50 mM cross-linking solution in which they both degraded rapidly. Strontium alginate, in turn, degraded less rapidly than the calcium alginate nanofiber counterparts.

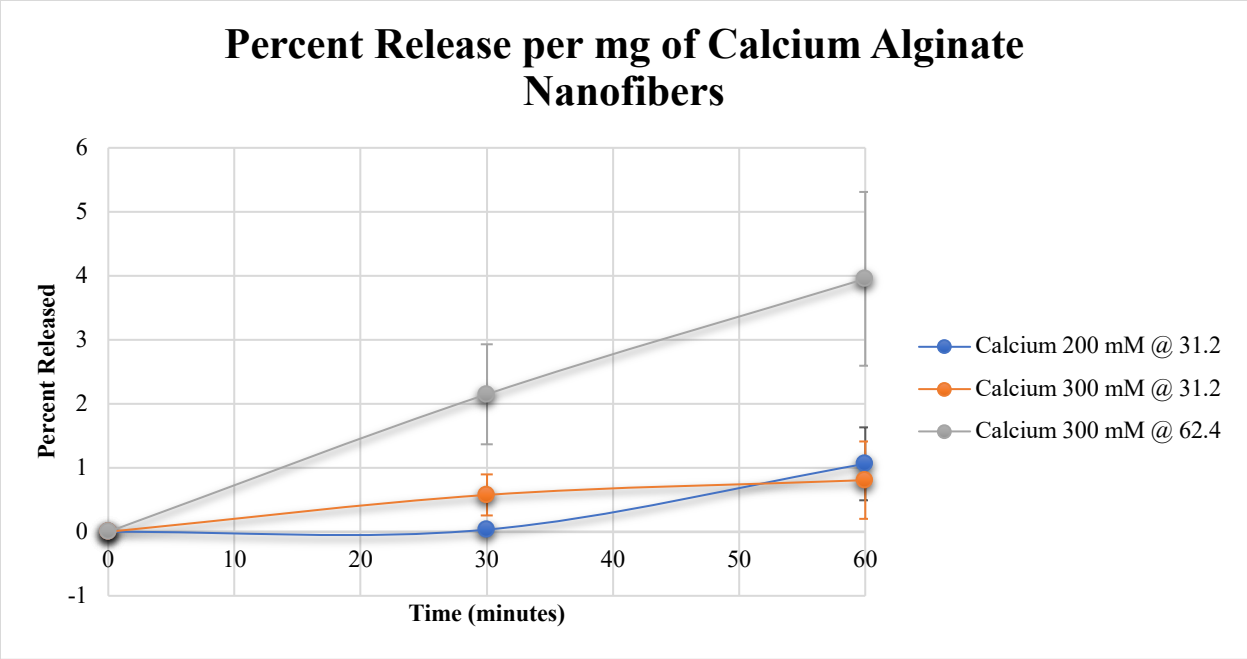

Figure 14: Methylene blue release profile of calcium cross-linked alginate nanofibers represented by the percent of total moles loaded onto the nanofibers release at various time points. Data stopping before the 180-minute mark represent nanofibers that degraded.

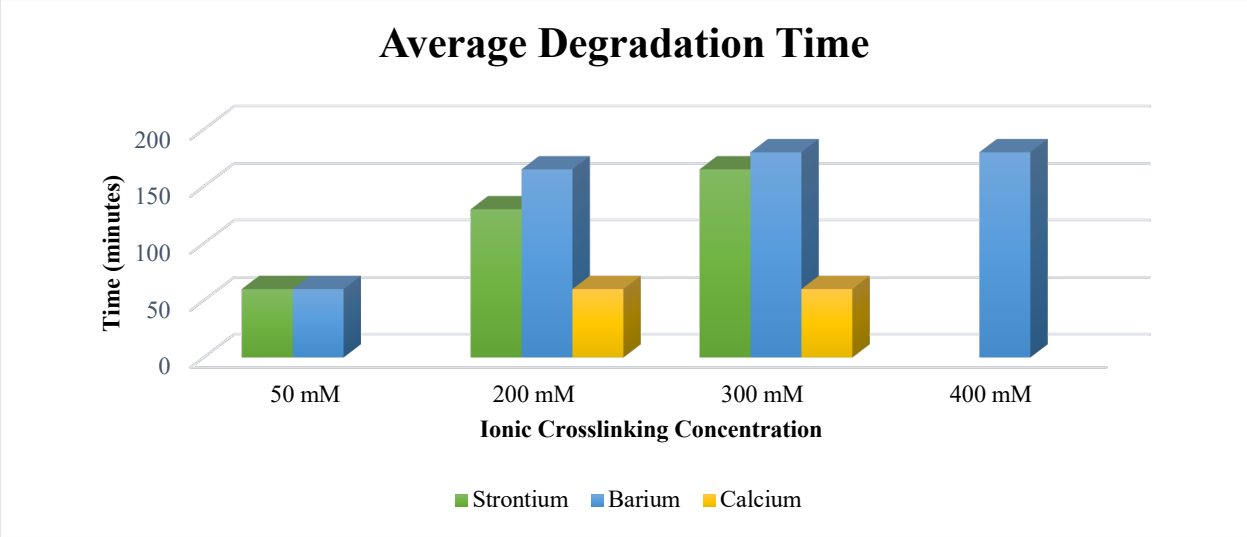

Figure 15: This statistical histogram depicts the average degradation time of differently cross-linked alginate nanofibers.

Discussion

The goal of this study was to identify the alginate cation cross-linked nanofiber with the highest loading efficiency for methylene blue, the highest capacity for moles loaded, had prolonged and steady release kinetics, and did not biodegrade before release was complete. The highest loading efficiency for methylene blue was observed for strontium 300 mM/31.2 µL at 59.9%. This means the strontium 300 mM/31.2 µL fiber absorbed the highest proportion of methylene blue present in the loading solution and subsequently wasted the least amount of methylene blue. This is ideal because the drugs of interest, Edaravone and Riluzole, are very expensive and it would be in both the industry's and patient's best interest to increase loading efficiency to minimize wasted drug product.[34,44] However, 59.9% is not near what would be optimal at an industrial level. Prompting the need for different configurations of alginate fibers to be tested. All strontium alginate nanofiber configurations outperformed their barium and calcium alginate nanofiber counterparts in loading efficiency. This trend became clearer when standardizing the alginate nanofibers down to the milligram. This standardization was necessary because triplicate samples of the same fiber often did not have the same exact weight and certainly did not have the same exact weight as the other two cation counterparts. The highest loading efficiency exhibited by a barium cross-linked alginate nanofiber was 35.2% for the 300 mM/31.2 µL configuration. Whereas, the highest loading efficiency exhibited by a calcium cross-linked alginate nanofiber was 24.9% by the 200 mM/31.2 µL configuration. Barium cross-linked alginate nanofibers often outperformed the calcium-cross-linked counterparts in loading efficiency. The trend of loading efficiency of strontium cross-linked alginate nanofibers had no clear pattern. However, when doubling the volume of methylene blue from 31.2 µL to 62.4 µL for the 300 mM strontium alginate nanofibers the loading efficiency reduced by about half. This

finding suggests that the 300 mM strontium alginate nanofibers had reached their maximum molar capacity at 31.2 µL and would only continue to load that same amount at 62.4 µL. The same phenomenon was exhibited by the 300 mM calcium alginate nanofibers. Barium alginate nanofibers did not have enough trials with the same type of nanofiber to make this comparison. However, it is likely that it reached its maximum ability to absorb methylene blue at 31.2 µL since the other two fibers exhibit that phenomena.

The number of moles loaded onto a milligram of alginate nanofiber is important to know for the appropriate dosing of drugs. The highest number of moles of methylene blue loaded onto a milligram of nanofiber was observed for 300 mM/31.2 µL strontium alginate at 2.79 nanomoles/mg or 83.7 nanomoles per 30 mg of fiber. The nanofiber could realistically be much bigger, however, it would still fall short of methylene blue's typical daily oral dosage of 625,293 nanomoles.[63] Further, the loading capability, if generalizable, would also fall short of Edaravone's daily dosage of about 344,431 nanomoles and Riluzole's daily dosage of about 426,987 nanomoles.[33,41]

It is important to note that the different modes of delivery, intrathecal administration versus the typical intravenous and oral administration, could potentially change the optimal drug dose. Strontium alginate nanofibers consistently loaded more nanomoles per mg of methylene blue than the barium and calcium alginate nanofiber counterparts. 300 mM strontium alginate nanofibers consistently loaded more moles than the strontium 200 mM counterpart. This could be due to tighter cross-linking within the higher concentration cross-linked fibers resulting in tighter nanopores in which methylene blue can enter. However, the same is not true for barium alginate nanofibers, which experienced maximal loading capacity for the 200 mM fibers and the 300 mM barium fibers and comparable molar loading in the 50 mM and 400 mM barium alginate

nanofibers. This could be due to enhanced cross-linking making the nanopores too small for methylene blue molecules to effectively enter for the 400 mM barium alginate nanofibers and too large for the 50 mM barium alginate nanofibers. Barium alginate nanofibers consistently loaded more nanomoles of methylene blue per milligram of fiber than their calcium counterparts. Both calcium alginate nanofibers, 200 mM and 300 mM loaded non-significantly different numbers of moles.

Release Profiles

The cumulative release profiles of the strontium, barium, and calcium alginate nanofibers revealed no obvious pattern. Nanofiber degradation inhibited data collection and release studies were stopped after significant nanofiber degradation inhibited the ability to collect samples for spectroscopy. For each cross-linking ion, strontium 200 mM/31.2 µL, barium 200 mM/62.4 µL, calcium 300 mM/62.4 µL, exhibited steady release. Barium 200 mM/62.4 µL exhibited the most ideal release profile of these. However, since the same fibers were analyzed at various loading concentrations it would be expected that the same nanofiber would have a similar release profile. This was not what was observed. For example, strontium 300 mM nanofibers release profiles were very dissimilar. The nanofiber loaded at 31.2 µL exhibited less total percentage release than the same nanofiber loaded at 62.4 µL. Similar trends are seen for barium 200 mM except that the fiber-loaded with 62.4 µL exhibited less total percentage release then when the fiber was loaded at 31.2 µL. On the other hand, nanofibers of different cross-linking concentrations displayed similar release characteristics. For example, barium 200 mM/7.8 µL, barium 400 mM/31.2 µL, and barium 300 mM/31.2 µL produced non-significantly different release profiles. Calcium 300 mM/31.2 µL and calcium 200 mM/31.2 µL yielded the same results. These seemingly random release patterns could be due to the inherently amorphous structure of the alginate nanofibers

which can be observed in Figure 5. Different aliquots of the fibers could have different levels of structure effecting their ability to load and release methylene blue. For this reason, in future studies, a higher number of replicate samples would be beneficial to reveal a pattern of release profiles within these nanofibers.

Degradation Profiles

The ideal degradation profile of these alginate nanofibers would involve nanofibers that remain their integrity just long enough to create a prolonged and sustained release of the loaded drug. To discern which nanofiber displayed the most ideal degradation pattern the average degradation times of the nine nanofiber types were measured. The two calcium-alginate nanofibers (200 mM, 300 mM) both degraded within an average of 60 minutes. The strontium alginate nanofibers exhibited a degradation pattern related to the cross-linking concentration. As the cross-linking concentration increased the average time of degradation also increased. The 50 mM strontium nanofibers degraded the fastest (60 minutes), followed by 200 mM (130 minutes), and 300 mM (165 minutes). This pattern is what was suspected for the nanofibers. As the amount of cross-linking increases, the structural integrity of the nanofibers should also increase leading to slower degradation times.[49] The barium alginate nanofibers also exhibited a cross-linking concentration-dependent relationship with degradation time. The barium alginate nanofibers 300 mM and 400 mM degraded the slowest after 180 minutes, followed by barium 200 mM (165 minutes) and barium 50 mM (60 minutes). However, higher concentrations can result in too high inhomogeneity of the network resulting in decreases in the network strength.[71] This limit was not observed in this study, but it is possible that at cross-linking concentrations higher than 400 mM the degradation times would start to decrease.

When comparing the degradation times among different cross-linking cations it was also thought that stronger ionic interactions between cations of higher charge density would result in stronger cross-linking to the negative carboxylic acid groups of alginate and longer degradation times. This was not the result. Calcium had the highest charge density of 52 C mm^{-3}, followed by strontium at 33 C mm^{-3}, and barium at 23 mm^{-3}. Interestingly, despite calcium having the highest charge density, it degraded the quickest and despite barium having the lowest charge density it had the highest integrity. Instead, the degradation profile seems to be more closely related to the atomic radius. Calcium has an atomic radius of 231 pm, strontium has an atomic radius of 255 pm, and barium has an atomic radius of 268 pm.[71] As atomic radius increased the fibers' degradation time also increased. Qualitatively, a more stable metal-ligand bond with barium exhibited a larger bond strength and a longer bond lifetime, whereas, strontium and calcium exhibited a less stable and more transient association. This is in line with alginate's proven affinity toward different divalent ions which has been shown to decrease in the following order: Ba > Sr > Ca.[71]

Limitations

There are some key limitations to this study. First, there are clear gaps in the data. Data for calcium 50 mM, calcium 400 mM, and strontium 400 mM nanofibers were not collected but would have been beneficial to the comparison of nanofibers above. Nanofibers for all cations cross-linked at 100 mM would have also added to a more complete characterization of these nanofibers. These missing fibers should have been analyzed at all three loading concentrations 12.2 nM, 48.8 nM, 97.5 nM to determine optimal loading concentration. Data for synthesized nanofibers at all different loading concentrations would have been beneficial for a more complete analysis and include: calcium 200 mM/12.2 nM, calcium 200 mM/97.5 nM, calcium

300 mM/12.2 nM, strontium 300 mM/12.2 nM, strontium 50 mM/48.4 nM, strontium 50 mM/97.5 nM, barium 50 mM/12.2 nM, barium 50 mM/97.5 nM, barium 300 mM/48.8 nM, barium 300 mM/12.2 nM, barium 300 mM/97.5 nM, barium 400 mM/12.2 nM, and barium 400 mM/97.5 nM.

The cumulative release profiles of the different alginate nanofibers produced no explainable patterns. In the laboratory oftentimes, the alginate nanofibers would look as though they released all loaded methylene blue. This was observable by the color change of the nanofibers from a dark blue to white. However, the release study analysis would show that only 20-30% of methylene blue was released. The phenomenon could be due to photobleaching of the dye. This interrupts data analysis significantly because the means of quantification of methylene blue is with UV-Vis spectrometry.

Third, these nanofibers were evaluated for their release profile of one non-FDA approved drug for the treatment of amyotrophic lateral sclerosis. Therefore, it does not mean that these nanofibers would exhibit similar loading efficiencies, molar capacities, release kinetics, or biodegradation patterns with Riluzole and Edaravone. Additionally, the nanofibers would also need to be examined for their release profiles of important macromolecules for neuroprotection such as brain-derived neurotrophic factor (BDNF), ciliary neurotrophic factor (CNTF) and insulin-like growth factors (IGF-1). This method of neurotrophic factor delivery has not been tested thus far and the addition of a scaffolding structure of alginate could further improve the beneficial effects of NFs. These molecules would likely have a different optimal alginate nanofiber configuration than the optimal alginate nanofiber used for smaller molecules such as methylene blue.

These nanofibers would eventually be evaluated *in vivo* and *in vitro*. Conditions in which *in vitro* drug release kinetics are tested and in which the nanofibers were tested in this study are performed in buffered saline. However, buffered saline (or phosphate-buffered solution) barely reflects the complexity of bodily fluids which contain proteins and lipids and can greatly challenge the stability of the nanocarriers. Consequently, it is often observed that drug release in serum complemented cell culture or in blood occurs much faster than predicted in buffered saline.[72] This could mean that nanofibers showing favorable release kinetics with sustained drug release between the minimal effective dose and below the minimal toxic dose in release studies such as this one, could have suboptimal release profiles when transitioned to *in vivo* systems. In the future, conditions for developing these alginate nanofibers and studying the release kinetics should more closely model the complexity of bodily fluids, particularly cerebrospinal fluid.

There is also a potential for the cross-linked cations to disrupt the biological system they are inserted into as the alginate nanofibers degrade and ions release into the surrounding environment. This is of particular concern for the cation barium. The permissible eight-hour exposure to barium is 0.5 mg/m^3 and the level that is immediately dangerous to life or health 50 mg/m^3.[73] The mechanisms involved in barium positioning are likely related to the metabolic control of potassium levels leading to hypokalemia.[73] Hypokalemia has adverse cardiovascular and muscular effects including tachycardia, changes in blood pressure, muscle weakness, and paralysis.[73] Therefore, the amount of barium present needs to be closely monitored during these release studies to ensure that barium cross-linked nanofibers do not lead to barium toxicity.

Further limitations to this study are due to the methods. Release studies were unable to occur over periods of more than three hours due to incomplete but extensive degradation of the nanofibers. This issue could have been avoided by increasing the amount of phosphate-buffered

solution and the sample vial size during release studies from 3 mL to 20 mL. This increase in volume would make it easier to obtain samples of the appropriate size (1-1.5 mL), with fewer pipette draws, that were free of degradation particulates for analysis by ultraviolet-visible spectrometry. Due to this limitation in vial size, degradation particulates could have been in samples that were analyzed in this study and potentially interfered with the quality of the data.

The methylene blue solution (Ward's Science) purchased for this study was designed for educational and teaching laboratories and had no certificate of analysis available. Therefore, this solution was most likely better suited for qualitative rather than quantitative studies. In future studies, the methylene blue purchased should be one that has a certificate of analysis such as those supplied by Spectrum Chemical MFG Corp.

Future Directions

Alginate is an adaptable biopolymer and its properties vary greatly based on source, cross-linking material, and preparation technique.[49] This study only explored one avenue: cross-linking three divalent cations in 1% alginate solutions. However, alginate has the ability to participate in covalent cross-linking and can be prepared at various concentrations to create different cross-linking densities and release profiles. These avenues should be explored for their applications to neural scaffolds and targeted drug release as it will be a continual challenge to match the physical properties of the alginate nanofiber to the particular application. One avenue that can be directly explored via an extension of this study is cross-linking alginate to mixtures calcium, strontium, and barium at different relative proportions to see if the release kinetics change favorably. Alginate solutions of different weight/volume content can also be investigated using the same cation cross-linking protocol as in this study. Further properties of alginate nanofibers can be explored through covalently cross-linking various reagents to the nanofiber,

such as poly(ethylene oxide). These different cross-linking polymers have the ability to significantly alter the release properties of the nanofibers. In fact, it is very difficult to reach the specified dosing targets for prolonged release of drugs using unipolymer nanofibers.[74] Other polymers that have seen success with alginate are poly(ethylene oxide), poly(ethylene glycol) and chitosan.[50] Poly(ethylene oxide) creates a less viscous alginate solution.[50] Poly(ethylene glycol) affects the mechanical properties and swelling of alginate nanofibers.[49] Whereas, chitosan cross-linked alginate results in a lower swelling ratio, increased cell adhesion, and increased cell proliferation compared to alginate nanofibers alone.[74] All of these properties can be utilized to further optimize alginate nanofibers.

More characterization of the various nanofibers also needs to take place to fully understand all of the contributing properties to the release kinetics and the integrity of the nanofiber mats. These physical properties of the nanofiber can be accessed by measurement of the density, uniformity, surface roughness, and mechanical strength.[74] Fiber properties such as morphology, arrangement, and surface features can also impact drug release kinetics.[74] These properties need to be included in the analysis of synthesized nanofibers in the future to better understand their effect on drug release. Scanning electron microscopy (SEM) and transmission electron spectroscopy (TEM) should be used to measure fiber size, size distribution, fiber alignment, and to visualize crystalline drug dispersed in the fibers.[74] X-ray photoelectron spectroscopy (XPS) can probe the surface chemistry of the nanofibers to quantify the amount of drug enriched at the fiber surface, a phenomenon that contributes to burst release kinetics.[74]

Acknowledgments

Dr. Ryan Tian for providing all necessary materials and instrumentation for the data collection and for developing the research question. Tian laboratory for support and advice on operating instrumentation. Parker Cole for developing the method and synthesizes all nanofibers evaluated. Bobbie Jean Sandidge and Clara Puente for assistance in release studies and data collection. This research was funded in part by the University of Arkansas Honors College Grant.

References

(1) Stroke, N. I. of N. D. and. Amyotrophic Lateral Sclerosis (ALS) Fac...e of Neurological Disorders and Stroke.pdf https://www.ninds.nih.gov/Disorders/Patient-Caregiver-Education/Fact-Sheets/Amyotrophic-Lateral-Sclerosis-ALS-Fact-Sheet.

(2) Motor Neuron Diseases Fact Sheet: National Institute of Neurological Disorders and Stroke (NINDS). *NIH Publication No. 12-5371*. 2012.

(3) Mayo Clinic (Institution/Organization). ALS. 2009, pp 84–94.

(4) van Es, M. A.; Hardiman, O.; Chio, A.; Al-Chalabi, A.; Pasterkamp, R. J.; Veldink, J. H.; van den Berg, L. H. Amyotrophic Lateral Sclerosis. *Lancet* **2017**, *390* (10107), 2084–2098. https://doi.org/10.1016/S0140-6736(17)31287-4.

(5) Symptoms and causes - Mayo Clinic.pdf https://www.mayoclinic.org/diseases-conditions/amyotrophic-lateral-sclerosis/symptoms-causes/syc-20354022.

(6) Abrahams, S.; Newton, J.; Niven, E.; Foley, J.; Bak, T. H. Screening for Cognition and Behaviour Changes in ALS. *Amyotroph. Lateral Scler. Front. Degener.* **2014**, *15* (1–2), 9–14. https://doi.org/10.3109/21678421.2013.805784.

(7) O'Toole, O.; Traynor, B. J.; Brennan, P.; Sheehan, C.; Frost, E.; Corr, B.; Hardiman, O. Epidemiology and Clinical Features of Amyotrophic Lateral Sclerosis in Ireland between 1995 and 2004. *J. Neurol. Neurosurg. Psychiatry* **2008**, *79* (1), 30–32. https://doi.org/10.1136/jnnp.2007.117788.

(8) Xu, L.; Liu, T.; Liu, L.; Yao, X.; Chen, L.; Fan, D.; Zhan, S.; Wang, S. Global Variation in Prevalence and Incidence of Amyotrophic Lateral Sclerosis: A Systematic Review and

Meta-Analysis. *J. Neurol.* **2019**. https://doi.org/10.1007/s00415-019-09652-y.

(9) McCombe, P. A.; Henderson, R. D. Effects of Gender in Amyotrophic Lateral Sclerosis. *Gend. Med.* **2010**, *7* (6), 557–570. https://doi.org/10.1016/j.genm.2010.11.010.

(10) Horton, D. K.; Mehta, P.; Antao, V. C. Quantifying a Nonnotifiable Disease in the United States. *Jama* **2014**, *312* (11), 1097. https://doi.org/10.1001/jama.2014.9799.

(11) Beard, J. D.; Steege, A. L.; Ju, J.; Lu, J.; Luckhaupt, S. E.; Schubauer-Berigan, M. K. Mortality from Amyotrophic Lateral Sclerosis and Parkinson's Disease among Different Occupation Groups — United States, 1985–2011. *Morb. Mortal. Wkly. Rep.* **2017**, *66* (27), 718–722. https://doi.org/10.15585/mmwr.mm6627a2.

(12) Vanacore, N.; Lehman, E. J.; Hein, M. J.; Baron, S. L.; Gersic, C. M. Neurodegenerative Causes of Death among Retired National Football League Players. *Neurology* **2013**, *80* (13), 1266–1267. https://doi.org/10.1212/01.wnl.0000428873.10254.b7.

(13) Schmidt, S.; Allen, K. D.; Loiacono, V. T.; Norman, B.; Stanwyck, C. L.; Nord, K. M.; Williams, C. D.; Kasarskis, E. J.; Kamel, F.; McGuire, V.; et al. Genes and Environmental Exposures in Veterans with Amyotrophic Lateral Sclerosis: The GENEVA Study: Rationale, Study Design and Demographic Characteristics. *Neuroepidemiology* **2008**, *30* (3), 191–204. https://doi.org/10.1159/000126911.

(14) Chiò, A.; Benzi, G.; Dossena, M.; Mutani, R.; Mora, G. Severely Increased Risk of Amyotrophic Lateral Sclerosis among Italian Professional Football Players. *Brain* **2005**, *128* (3), 472–476. https://doi.org/10.1093/brain/awh373.

(15) McGuire, V.; Longstreth, W. T.; Nelson, L. M.; Koepsell, T. D.; Checkoway, H.; Morgan,

M. S.; Van Belle, G. Occupational Exposures and Amyotrophic Lateral Sclerosis: A Population- Based Case-Control Study. *Am. J. Epidemiol.* **1997**, *145* (12), 1076–1088. https://doi.org/10.1093/oxfordjournals.aje.a009070.

(16) Beard, J. D.; Kamel, F. Military Service, Deployments, and Exposures in Relation to Amyotrophic Lateral Sclerosis Etiology and Survival. *Epidemiol. Rev.* **2015**, *37* (1), 55–70. https://doi.org/10.1093/epirev/mxu001.

(17) Sutedja, N. A.; Veldink, J. H.; Fischer, K.; Kromhout, H.; Heederik, D.; Huisman, M. H. B.; Wokke, J. H. J.; Van Den Berg, L. H. Exposure to Chemicals and Metals and Risk of Amyotrophic Lateral Sclerosis: A Systematic Review. *Amyotroph. Lateral Scler.* **2009**, *10* (5–6), 302–309. https://doi.org/10.3109/17482960802455416.

(18) Wang, H.; O'reilly, E.; Weisskopf, M. G.; Logroscino, G.; McCullough, M. L.; Thun, M.; Schatzkin, A.; Kolonel, L. N.; Ascheerio, A. Smoking and Risk of Amyotrophic Lateral Sclerosis: A Pooled Analysis of Five Prospective Cohorts. *Proteins* **2010**, *78* (8), 1825–1846. https://doi.org/10.1001/archneurol.2010.367.Smoking.

(19) Arthur, K. C.; Calvo, A.; Price, T. R.; Geiger, J. T.; Chiò, A.; Traynor, B. J. Projected Increase in Amyotrophic Lateral Sclerosis from 2015 to 2040. *Nat. Commun.* **2016**, *7*, 1–6. https://doi.org/10.1038/ncomms12408.

(20) Baeza-Yates, R.; Sangal, P. M.; Villoslada, P. Burden of Neurological Diseases in the US Revealed by Web Searches. *PLoS One* **2017**, *12* (5), 1–9. https://doi.org/10.1371/journal.pone.0178019.

(21) López-Bastida, J.; Perestelo-Pérez, L.; Montón-Álvarez, F.; Serrano-Aguilar, P.; Alfonso-Sanchez, J. L. Social Economic Costs and Health-Related Quality of Life in Patients with

Amyotrophic Lateral Sclerosis in Spain. *Amyotroph. Lateral Scler.* **2009**, *10* (4), 237–243. https://doi.org/10.1080/17482960802430781.

(22) Schepelmann, K.; Winter, Y.; Spottke, A. E.; Claus, D.; Grothe, C.; Schröder, R.; Heuss, D.; Vielhaber, S.; Mylius, V.; Kiefer, R.; et al. Socioeconomic Burden of Amyotrophic Lateral Sclerosis, Myasthenia Gravis and Facioscapulohumeral Muscular Dystrophy. *J. Neurol.* **2010**, *257* (1), 15–23. https://doi.org/10.1007/s00415-009-5256-6.

(23) Renton, A. E.; Chiò, A.; Traynor, B. J.; Neurosci, N. State of Play in Amyotrophic Lateral Sclerosis Genetics HHS Public Access Author Manuscript. *Nat Neurosci* **2014**, *17* (1), 17–23. https://doi.org/10.1038/nn.3584.

(24) Rosen, D. Mutations in Cu/Zn Superoxide Dismutase Gene Are Associated with Familial Amyotrophic Lateral Sclerosis. *Nature* **1993**, *364* (6435), 362–362. https://doi.org/10.1038/364362c0.

(25) Prasad, A.; Bharathi, V.; Sivalingam, V.; Girdhar, A.; Patel, B. K. Molecular Mechanisms of TDP-43 Misfolding and Pathology in Amyotrophic Lateral Sclerosis. *Front. Mol. Neurosci.* **2019**, *12* (February), 1–36. https://doi.org/10.3389/fnmol.2019.00025.

(26) An, H.; Skelt, L.; Notaro, A.; Highley, J. R.; Fox, A. H.; La Bella, V.; Buchman, V. L.; Shelkovnikova, T. A. ALS-Linked FUS Mutations Confer Loss and Gain of Function in the Nucleus by Promoting Excessive Formation of Dysfunctional Paraspeckles. *Acta Neuropathol. Commun.* **2019**, *7* (1), 7. https://doi.org/10.1186/s40478-019-0658-x.

(27) Laurin, N.; Brown, J. P.; Morissette, J.; Raymond, V. Recurrent Mutation of the Gene Encoding Sequestosome 1 (SQSTM1/P62) in Paget Disease of Bone. *Am. J. Hum. Genet.* **2002**, *70* (6), 1582–1588. https://doi.org/10.1086/340731.

(28) Deng, H.; Chen, W.; Hong, S.; Boycott, K. M.; George, H.; Siddique, N.; Yang, Y.; Fecto, F.; Shi, Y.; Zhai, H.; et al. Mutations in UBQLN2 Cause Dominant X-Linked Juvenile and Adult Onset ALS and ALS/Dementia. **2012**, *477* (7363), 211–215. https://doi.org/10.1038/nature10353.Mutations.

(29) Fratta, P.; Mizielinska, S.; Nicoll, A. J.; Zloh, M.; Fisher, E. M. C.; Parkinson, G.; Isaacs, A. M. C9orf72 Hexanucleotide Repeat Associated with Amyotrophic Lateral Sclerosis and Frontotemporal Dementia Forms RNA G-Quadruplexes. *Sci. Rep.* **2012**, *2*, 1–6. https://doi.org/10.1038/srep01016.

(30) Martin R Turner, PhDa, Prof Orla Hardiman, MDb, Michael Benatar, DPhilc, Prof Benjamin R Brooks, MDd, Prof Adriano Chio, MDe, Prof Mamede de Carvalho, MDf, Prof Paul G Ince, MDg, Cindy Lin, PhDh, Robert G Miller, MDi, Prof Hiroshi Mitsumoto, MDj, Prof Gar, Ds.; A. Controversies and Priorities in Amyotrophic Lateral Sclerosis. *Physiol. Behav.* **2016**, *176* (1), 139–148. https://doi.org/10.1016/j.physbeh.2017.03.040.

(31) Petrov, D.; Mansfield, C.; Moussy, A.; Hermine, O. ALS Clinical Trials Review: 20 Years of Failure. Are We Any Closer to Registering a New Treatment? *Front. Aging Neurosci.* **2017**, *9* (MAR), 1–11. https://doi.org/10.3389/fnagi.2017.00068.

(32) Rothstein, J. D. Excitotoxic Mechanisms in the Pathogenesis of Amyotrophic Lateral Sclerosis. *Adv. Neurol.* **1995**, *68*, 7–27.

(33) Miller, R. G.; Mitchell, J. D.; Lyon, M.; Moore, D. H. Riluzole for Amyotrophic Lateral Sclerosis (ALS)/Motor Neuron Disease (MND). *Amyotroph. Lateral Scler. Other Mot. Neuron Disord.* **2003**, *4* (3), 191–206. https://doi.org/10.1080/14660820310002601.

(34) Kasarskis. Cost of Riluzole.Pdf. ALS Association.

(35) Zhao, W.; Beers, D. R.; Appel, S. H. Immune-Mediated Mechanisms in the Pathoprogression of Amyotrophic Lateral Sclerosis. *J. Neuroimmune Pharmacol.* **2013**, *8* (4), 888–899. https://doi.org/10.1007/s11481-013-9489-x.

(36) Trias, E.; King, P. H.; Si, Y.; Kwon, Y.; Varela, V.; Ibarburu, S.; Kovacs, M.; Moura, I. C.; Beckman, J. S.; Hermine, O.; et al. Mast Cells and Neutrophils Mediate Peripheral Motor Pathway Degeneration in ALS. *JCI insight* **2018**, *3* (19). https://doi.org/10.1172/jci.insight.123249.

(37) Mora, J. S.; Genge, A.; Chio, A.; Estol, C. J.; Chaverri, D.; Hernández, M.; MarÍn, S.; Mascias, J.; Rodriguez, G. E.; Povedano, M.; et al. Masitinib as an Add-on Therapy to Riluzole in Patients with Amyotrophic Lateral Sclerosis: A Randomized Clinical Trial. *Amyotroph. Lateral Scler. Front. Degener.* **2019**, *0* (0), 1–10. https://doi.org/10.1080/21678421.2019.1632346.

(38) Barber, S. C.; Mead, R. J.; Shaw, P. J. Oxidative Stress in ALS: A Mechanism of Neurodegeneration and a Therapeutic Target. *Biochim. Biophys. Acta - Mol. Basis Dis.* **2006**, *1762* (11–12), 1051–1067. https://doi.org/10.1016/j.bbadis.2006.03.008.

(39) Cohen, T. J.; Hwang, A. W.; Restrepo, C. R.; Yuan, C. X.; Trojanowski, J. Q.; Lee, V. M. Y. An Acetylation Switch Controls TDP-43 Function and Aggregation Propensity. *Nat. Commun.* **2015**, *6*, 1–13. https://doi.org/10.1038/ncomms6845.

(40) Vance, C.; Scotter, E. L.; Nishimura, A. L.; Troakes, C.; Mitchell, J. C.; Kathe, C.; Urwin, H.; Manser, C.; Miller, C. C.; Hortobágyi, T.; et al. ALS Mutant FUS Disrupts Nuclear Localization and Sequesters Wild-Type FUS within Cytoplasmic Stress Granules. *Hum.*

Mol. Genet. **2013**, *22* (13), 2676–2688. https://doi.org/10.1093/hmg/ddt117.

(41) Luo, L.; Song, Z.; Li, X.; Huiwang; Zeng, Y.; Qinwang; Meiqi; He, J. Efficacy and Safety of Edaravone in Treatment of Amyotrophic Lateral Sclerosis—a Systematic Review and Meta-Analysis. *Neurol. Sci.* **2019**, *40* (2), 235–241. https://doi.org/10.1007/s10072-018-3653-2.

(42) Watanabe, T.; Yuki, S.; Egawa, M.; Nishi, H. Protective Effects of MCI-186 on Cerebral Ischemia: Possible Involvement of Free Radical Scavenging and Antioxidant Actions. *Journal of Pharmacology and Experimental Therapeutics*. 1994, pp 1597–1604.

(43) Yoshino, H.; Kimura, A. Investigation of the Therapeutic Effects of Edaravone, a Free Radical Scavenger, on Amyotrophic Lateral Sclerosis (Phase II Study). *Amyotroph. Lateral Scler.* **2006**, *7* (4), 247–251. https://doi.org/10.1080/17482960600881870.

(44) Chang, A.; Ross, M. A. Edaravone: Costs versus Benefits | Clinical Neurology News.

(45) Henriques, A.; Pitzer, C.; Schneider, A. Neurotrophic Growth Factors for the Treatment of Amyotrophic Lateral Sclerosis: Where Do We Stand? *Front. Neurosci.* **2010**, *4* (JUN), 1–14. https://doi.org/10.3389/fnins.2010.00032.

(46) Bemelmans, A. P.; Husson, I.; Jaquet, M.; Mallet, J.; Kosofsky, B. E.; Gressens, P. Lentiviral-Mediated Gene Transfer of Brain-Derived Neurotrophic Factor Is Neuroprotective in a Mouse Model of Neonatal Excitotoxic Challenge. *J. Neurosci. Res.* **2006**, *83* (1), 50–60. https://doi.org/10.1002/jnr.20704.

(47) Xing, M.; Cao, Q.; Wang, Y.; Xiao, H.; Zhao, J.; Zhang, Q.; Ji, A.; Song, S. Advances in Research on the Bioactivity of Alginate Oligosaccharides. *Mar. Drugs* **2020**, *18*.

https://doi.org/10.3390/md18030144.

(48) Kevin Range, and D. M. Y. A. M. Controlled Drug Release from Pharmaceutical Nanocarriers Jinhyun. *Chem. Enigneering Sci. J.* **2015**, *125*, 75–84. https://doi.org/10.1038/jid.2014.371.

(49) Lee, K. Y.; Mooney, D. J. Alginate: Properties and Biomedical Applications. *Prog. Polym. Sci.* **2012**, *37* (1), 106–126. https://doi.org/10.1016/j.progpolymsci.2011.06.003.

(50) Bhattarai, N.; Li, Z.; Edmondson, D.; Zhang, M. Alginate-Based Nanofibrous Scaffolds: Structural, Mechanical, and Biological Properties. *Adv. Mater.* **2006**, *18* (11), 1463–1467. https://doi.org/10.1002/adma.200502537.

(51) Zhou, R.; Shi, X. Y.; Bi, D. C.; Fang, W. S.; Wei, G. Bin; Xu, X. Alginate-Derived Oligosaccharide Inhibits Neuroinflammation and Promotes Microglial Phagocytosis of β-Amyloid. *Mar. Drugs* **2015**, *13* (9), 5828–5846. https://doi.org/10.3390/md13095828.

(52) Eftekharzadeh, B.; Khodagholi, F.; Abdi, A.; Maghsoudi, N. Alginate Protects NT2 Neurons against H2O2-Induced Neurotoxicity. *Carbohydr. Polym.* **2010**, *79* (4), 1063–1072. https://doi.org/10.1016/j.carbpol.2009.10.040.

(53) Yamamoto, Y.; Kurachi, M.; Yamaguchi, K.; Oda, T. Stimulation of Multiple Cytokine Production in Mice by Alginate Oligosaccharides Following Intraperitoneal Administration. *Carbohydr. Res.* **2007**, *342* (8), 1133–1137. https://doi.org/10.1016/j.carres.2007.02.015.

(54) Xu, X.; Bi, D.; Wu, X.; Wang, Q.; Wei, G.; Chi, L.; Jiang, Z.; Oda, T.; Wan, M. Unsaturated Guluronate Oligosaccharide Enhances the Antibacterial Activities of

Macrophages. *FASEB J.* **2014**, *28* (6), 2645–2654. https://doi.org/10.1096/fj.13-247791.

(55) Shoichet, M. S.; Li, R. H.; White, M. L.; Winn, S. R. Stability of Hydrogels Used in Cell Encapsulation: An in Vitro Comparison of Alginate and Agarose. *Biotechnol. Bioeng.* **1996**, *50* (4), 374–381. https://doi.org/10.1002/(SICI)1097-0290(19960520)50:4<374::AID-BIT4>3.0.CO;2-I.

(56) Al-Shamkhani, A.; Duncan, R. Radioiodination of Alginate via Covalently-Bound Tyrosinamide Allows Monitoring of Its Fate In Vivo. *J. Bioact. Compat. Polym.* **1995**, *10* (1), 4–13.

(57) Rabbany, S. Y.; Pastore, J.; Yamamoto, M.; Miller, T.; Rafii, S.; Aras, R.; Penn, M. Continuous Delivery of Stromal Cell-Derived Factor-1 from Alginate Scaffolds Accelerates Wound Healing. *Cell Transplant.* **2010**, *19* (4), 399–408. https://doi.org/10.3727/096368909X481782.

(58) Borselli, C.; Storrie, H.; Benesch-Lee, F.; Shvartsman, D.; Cezar, C.; Lichtman, J. W.; Vandenburgh, H. H.; Mooney, D. J. Functional Muscle Regeneration with Combined Delivery of Angiogenesis and Myogenesis Factors. *Proc. Natl. Acad. Sci. U. S. A.* **2010**, *107* (8), 3287–3292. https://doi.org/10.1073/pnas.0903875106.

(59) Buket Basmanav, F.; Kose, G. T.; Hasirci, V. Sequential Growth Factor Delivery from Complexed Microspheres for Bone Tissue Engineering. *Biomaterials* **2008**, *29* (31), 4195–4204. https://doi.org/10.1016/j.biomaterials.2008.07.017.

(60) Prang, P.; Müller, R.; Eljaouhari, A.; Heckmann, K.; Kunz, W.; Weber, T.; Faber, C.; Vroemen, M.; Bogdahn, U.; Weidner, N. The Promotion of Oriented Axonal Regrowth in the Injured Spinal Cord by Alginate-Based Anisotropic Capillary Hydrogels. *Biomaterials*

2006, *27* (19), 3560–3569. https://doi.org/10.1016/j.biomaterials.2006.01.053.

(61) Sufan, W.; Suzuki, Y.; Tanihara, M.; Ohnishi, K.; Suzuki, K.; Endo, K.; Nishimura, Y. Sciatic Nerve Regeneration through Alginate with Tubulation or Nontubulation Repair in Cat. *J. Neurotrauma* **2001**, *18* (3), 329–338. https://doi.org/10.1089/08977150151070991.

(62) Huang, D.; Lin, C.; Wen, X.; Gu, S.; Zhao, P. A Potential Nanofiber Membrane Device for Filling Surgical Residual Cavity to Prevent Glioma Recurrence and Improve Local Neural Tissue Reconstruction. *PLoS One* **2016**, *11* (8), 1–15. https://doi.org/10.1371/journal.pone.0161435.

(63) Schirmer, R. H.; Adler, H.; Pickhardt, M.; Mandelkow, E. "Lest We Forget You - Methylene Blue..." *Neurobiol. Aging* **2011**, *32* (12), 2325.e7-2325.e16. https://doi.org/10.1016/j.neurobiolaging.2010.12.012.

(64) Wischik, C. M.; Bentham, P.; Wischik, D. J.; Seng, K. M. Tau Aggregation Inhibitor (TAI) Therapy with Rember Arrests Disease Progression in Mild and Moderate Alzheimer's Disease over 50 Weeks. *Alzheimer's Dement. J. Alzheimer's Assoc.* **2008**, *4* (4), T167.

(65) Necula, M.; Breydo, L.; Milton, S.; Kayed, R.; Van Der Veer, W. E.; Tone, P.; Glabe, C. G. Methylene Blue Inhibits Amyloid Aβ Oligomerization by Promoting Fibrillization. *Biochemistry* **2007**, *46* (30), 8850–8860. https://doi.org/10.1021/bi700411k.

(66) Yamashita, M.; Nonaka, T.; Arai, T.; Kametani, F.; Buchman, V. L.; Ninkina, N.; Bachurin, S. O.; Akiyama, H.; Goedert, M.; Hasegawa, M. Methylene Blue and Dimebon Inhibit Aggregation of TDP-43 in Cellular Models. *FEBS Lett.* **2009**, *583* (14), 2419–2424. https://doi.org/10.1016/j.febslet.2009.06.042.

(67) Riha, P. D.; Bruchey, A. K.; Echevarria, D. J.; Gonzalez-Lima, F. Memory Facilitation by Methylene Blue: Dose-Dependent Effect on Behavior and Brain Oxygen Consumption. *Eur. J. Pharmacol.* **2005**, *511* (2–3), 151–158. https://doi.org/10.1016/j.ejphar.2005.02.001.

(68) Peter, C.; Hongwan, D.; Küpfer, A.; Lauterburg, B. H. Pharmacokinetics and Organ Distribution of Intravenous and Oral Methylene Blue. *Eur. J. Clin. Pharmacol.* **2000**, *56* (3), 247–250. https://doi.org/10.1007/s002280000124.

(69) Walter-Sack, I.; Rengelshausen, J.; Oberwittler, H.; Burhenne, J.; Mueller, O.; Meissner, P.; Mikus, G. High Absolute Bioavailability of Methylene Blue given as an Aqueous Oral Formulation. *European Journal of Clinical Pharmacology*. 2009, pp 179–189. https://doi.org/10.1007/s00228-008-0563-x.

(70) Grant M. Gonzalez, Luke A. MacQueen, Johan U. Lind, Stacey A. Fitzgibbons, Christophe O. Chantre, Isabelle Huggler, Holly M. Golecki, Josue A. Goss, K. K. P. Production of Synthetic, Para-Aramid and Biopolymer Nanofibers by Immersion Rotary Jet-Spinning. *Macromol. Mater. Eng.* **2017**, *302* (6), 1–11. https://doi.org/10.1002/mame.201600365.

(71) Zhou, Q.; Kang, H.; Bielec, M.; Wu, X.; Cheng, Q.; Wei, W.; Dai, H. Influence of Different Divalent Ions Cross-Linking Sodium Alginate-Polyacrylamide Hydrogels on Antibacterial Properties and Wound Healing. *Carbohydr. Polym.* **2018**, *197* (July 2017), 292–304. https://doi.org/10.1016/j.carbpol.2018.05.078.

(72) Liu, K. C.; Yeo, Y. Extracellular Stability of Nanoparticulate Drug Carriers. *Arch. Pharm. Res.* **2014**, *37* (1), 16–23. https://doi.org/10.1007/s12272-013-0286-0.

(73) Agency for Toxic Substances and Disease Registry (Instituion). Toxicological Profile for Barium and Barium Compounds. *Agency toxic Subst. Dis. Regist.* **2007**, No. August, 184.

(74) Ahn, H.; Weaver, M.; Lyon, D.; Choi, E.; Fillingim, R. B. Current Strategies for Sustaining Drug Release Form Electrospun Nanofibers. *Physiol. Behav.* **2017**, *176* (10), 139–148. https://doi.org/10.1016/j.physbeh.2017.03.040.

Appendix

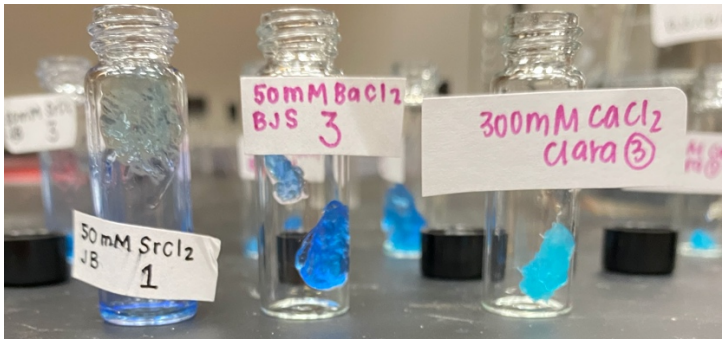

Figure 16: comparison of 50 mM Strontium, 50 mM Barium, and 300 mM calcium alginate nanofibers macroscopic features after 12 hours of incubation in methylene blue.

Figure 17: Comparison of 300 mM Barium alginate nanofibers loaded with methylene blue (top) versus not loaded (bottom).

Figure 18: comparison of 50 mM Strontium, 50 mM barium, and 300 mM calcium cross-linked alginate nanofibers macroscopic morphological features after a 12-hour incubation period in methylene blue.

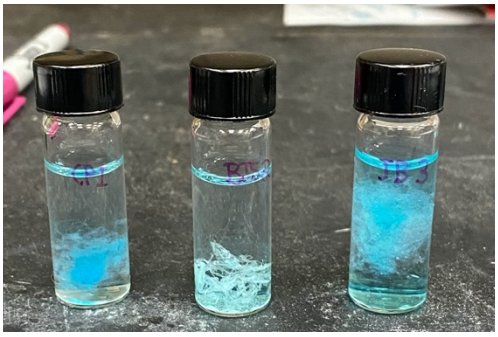

Figure 19: Comparison of the macroscopic morphological properties of Calcium 200 mM cross-linked alginate (left), barium 400 mM cross-linked alginate (middle), and strontium 200 mM cross-linked alginate nanofiber (right) in PBS solution at the start of a drug release study.